Authors replies to the interactive comments of anonymous referee #1 (30 May 2019) on “High-resolution under-water laser spectrometer sensing provides new insights to methane distribution at an Arctic seepage site” by Pär Jansson et al.

RC: denotes referee’s comments

AR: denotes authors’ reply

MC: denotes manuscript changes

RC: General Comments: As pointed out by the authors this is a FIRST, and hopefully the instrumentation described will enable a new era of high-quality data to be gathered for ocean and climate studies. The authors can document and quantify both the temporal and spatial heterogeneity of CH4 concentrations in the water column. That such heterogeneity exists is not new, but that it can be quantitatively studied is new. So far technology has limited researchers to either discrete sampling or use of sensors with long response times both making it practically impossible to describe the heterogeneities described in the present study. Coarse data allows for coarse models and budgets. This becomes evident in the data analysis presented. Although the data is high resolution, general applicability of the method for inventory (budgets) studies requires a large amount of auxiliary data (current, CTD, TS, background/reference measurements). But this is the everyday challenge of the oceanographer (and modeller). The data will allow for substantial discussions within the modelling community. Hopefully, in the future we will see sensors with similar characteristics to that of the "MILS" fitted to groups/swarms of AUV’s that can do concurrent sampling and monitoring of larger regions. This could enable true high-resolution characterization of a region of interest and enable high resolution modelling of CH4 dispersion dynamics. Such data will need to be collected in order to be able to use "bottom up" studies to build confidence in "top down" data and models used for inventory monitoring at the ocean and climate scales.

AR: Thank you for taking the time and effort to read and comment on our manuscript. You acknowledge the need for this kind of research, and recognize the hardship of acquiring useful data, even with the new advanced technology. We appreciate your comments, which we believe has improved the manuscript. We agree that this type of high-resolution measurements is the beginning of a new era of Oceanographic surveys, and that more data, both in time and space, is needed for a broader understanding.

RC: Specific comments: Page 5 L114-117: Where was the pump inlet located? This is not described in the paper nor in Grilli et al. 2018. A schematic is provided of the membrane assembly in SI3 of Grilli et al. 2018. Page 6 L121-129:

AR: The water circulation pump (Seabird SBE 5T) was located at the bottom of the MILS instrument approx. 25 cm away from the membrane assembly block. Short sections of ½" hose and a T-piece were used to connect the pump outlet to the membrane block inlets. The pump inlet was shielded with a cover and a fine mess to avoid ingress of particles and/or bubbles.

MC: This information was added to the text in lines 121–123.

RC: Regarding the position correction. A cylinder of height and width of the MILS probe was used. The assembly in Figure 1b show that the CTD, Battery and commercial CH4 sensor is far from symmetric, and the drag of these side mounted addons should probably have been accounted for in the position correction. These addons could also lead to a wobbling and rotation of the assembly. Was this monitored by onboard IMU sensors (inertial measurement unit)?

AR: For the position correction, a cylinder shape was used with a height and diameter equivalent to the displacement/buoyancy of the total assembly of instruments (i.e. not just the height and width of the MILS). This ensured that the simulated buoyancy of the total assembly was as close to reality as possible to allow for the (unknown) drag coefficient to be determined by making the simulation match with all the other known parameters such as instrument depth, cable length, ship speed, ship direction, and currents. It is unknown how stable the instrument assembly was while being towed, but wobble and/or rotation would have no significant effect on the measurements. No IMU sensors were used to monitor the movement of the assembly during profiling.

MC: This information has now been added to the discussion in lines 364–365

RC: Section 3.1 Water properties It is not clear from the text that the current information is derived from data obtained simultaneously with the CH4 measurements. This is however stated in Jansson (2019) Figure 8b.

AR: We agree that this should be more clearly stated. We added a note on that in the manuscript

MC: lines 204–206 state the above.

RC: When interpreting the inclination of the flairs is flair inclination perpendicular to the ship motion taken into account?

AR: The split-beam echosounder (Simrad EK60) resolves the location of scattering objects in 3 dimensions, but the echosounder swath width (~7°) will set a limit to the positions of the scattering objects. Particularly, in the direction perpendicular to the ships' movement, the bubbles may easily escape the beam if the current carries them across the ship trajectory. During our survey, the heading of the ship is biased towards the N/S and S/N direction, and it is therefore possible for flares to extend more in that direction. However, careful investigation of

the flare data shows that the flares detected during cross-slope sailing have very small east-west components even though they could potentially extend across-slope within the echosounder beam. We are therefore convinced that our flare-inferred currents represent real currents. Furthermore, ocean currents generally flow along isobaths, and the streamlines determined by potential vorticity conservation, follow the isobaths closely in this area Nilsen et al. (2016).

RC: There can of course be unknown sources of the CH4, but there is mention of WSC meandering, and negligible tidal effects. Have typical eddy sizes been characterized? The time between transect lines 1 and 5 are by rough estimation 12 hrs i.e. roughly one tidal period. The whole cruise was two tidal periods. What is the direction of the tidal flow in this region? Both eddy size and tidal currents could result in noticeable advection over a 12-hr period.

AR: Eddies are difficult to observe with sparse observations, but high resolution modelling suggests that mesoscale (a few km) eddies are important for transport of water properties across the slope in the study area. Mesoscale and smaller eddies form on each side of the WSC core, which also meanders off- and onshore of our study site (Hattermann et al., 2016, supplementary information). This process obviously affects also methane concentrations, which could appear high or low without other obvious explanations. We do not discard the possibility that eddies transport CH_4 enriched water in ways that we cannot predict without perfect knowledge of the velocity field. We simply put forward the possibility that unknown sources could be tracked with the new instrument. The CH_4 enriched water that we observe in the northern part of line 3, not explained by acoustically observed flares, was accompanied with a TS anomaly. This suggest intrusion of a different water mass, but not all of the intrusion was enriched with CH_4. Possibly, this is eddy induced, or it could be a result of bottom Ekman transport.

MC: We added the possibility for eddies in the discussion (line 385).

AR: The survey lasted for three days (October 21st – 23rd). The probe was deployed each morning around 10 AM, and was measuring continuously for 4, 9, and 10 hours respectively. The tidally driven currents in the area range between -1 and 1 cm s^{-1} in both the east and north directions. The probe was deployed at the approximate same tidal state and the modelled tides during the deployments were 0–1 vs -0.5–0.5 cm s^{-1} in the N and E direction respectively.

RC: Page 13 L267: with the given speed of the cruise and the response time of the instrument (15 sec), spatial resolution is of the order 10m. However, how does the instrument obtain a measurement? Is it by continuous

flow at a given flow rate over the membrane, or does it work in a batch mode with discrete samples passed over the membrane unit?

AR Both the water flow over the membranes and the gas flows inside the instrument are continuous and constant during the cast/deployment.

RC: Page 13 L280: What is the reasoning behind scaling up the flair by 40%? Can the authors justify this quantitatively?

AR: The 40% upscaling is based on the “dissolution function” or “non-dimensional source-function” (sect 2.6), which shows that a large portion of the initial CH_4 is already lost from the bubbles when we observe them with the echosounder in the layer 5 – 10 masf.

MC: The upscaling due to dissolution is now better explained in line 292.

RC: Technical corrections: Page 4 – L62-75 A map/graphic could be included for illustration if authors have access to graphical assistance.

AR: An illustration with currents carrying the different water masses would be nice, but it is outside the scope of this paper to produce an infographic on water mass movements. The physical oceanography is well documented in the referenced papers and we do not wish to review them extensively in our manuscript. To partly meet your suggestion, we added the main controlling ocean currents in figure 1a (inset map). Water mass classifications are found in the TS-diagram in Figure 2b and 2c.

MC: Figure 1 was updated and now indicates the dominating currents.

RC: Page 4 – L80 and L95-97: purely cosmetic but I like it when lists come in the same order, e.g. temp, salinity and concentration.

AR: We agree.

MC: Order of parameters changed in line 102.

RC: Page 7 – L150-180: I feel that the presentation in paragraphs 2.5 and 2.6 could benefit from a graphic illustrating the computational domains. I believe that this will aid the reader in understanding and conceptualizing the differences between the two methods better.

AR We posted a supplementary containing a schematic showing the control volume and the 2D model, which indicates the included processes for easier understanding.

MC: Fig. SI 1 was added in the supplementary document.

RC: Figure 2: Second line: it should read "Gibbs seawater package". In the last line: the mean bubble rise velocity is 23 cm s-1, could you provide the mean bubble size as well?

AR: Thanks for noticing that. We corrected the caption for figure 2. We added the bubble size distribution.

MC: Manusript changed accordingly. Bubble size distribution in line 159.

RC: Figure 7: The figure would be much easier to read if it was in colour.

AR: Ok.

MC: Figure 7 and its caption has been updated accordingly.

Hattermann, T., Isachsen, P. E., Appen, W. J., Albretsen, J., and Sundfjord, A.: Eddy-driven recirculation of Atlantic Water in Fram Strait, Geophys. Res. Lett., 43, 3406-3414, 2016.
Nilsen, F., Skogseth, R., Vaardal-Lunde, J., and Inall, M.: A Simple Shelf Circulation Model: Intrusion of Atlantic Water on the West Spitsbergen Shelf, Journal of Physical Oceanography, 46, 1209-1230, 10.1175/jpo-d-15-0058.1, 2016.

Authors replies to the interactive comments of anonymous referee #2 (5 June 2019) on "High-resolution under-water laser spectrometer sensing provides new insights to methane distribution at an Arctic seepage site" by Pär Jansson et al.

RC: denotes referee's comments

AR: denotes authors' reply

MC: denotes manuscript changes

RC: General comments The manuscript describes how a new technology/sensor can improve our knowledge on the distribution and the dynamics of CH4 over an Arctic seep area. This technology uses a laser spectrometer and a membrane inlet to extract the gas from the aqueous phase. The manuscript is clearly written, results and discussion are well presented, although a bit confusing when it gets to the description of the models (a schematic/conceptual model would have been appreciated). Without any doubt, the lack of in situ, high-resolution measurements of methane in marine environments makes difficult to fully understand their role as a source and/or a sink of methane. This is probably for this reason the contribution of the oceans to the global methane budget has been underestimated. So every effort to develop and test new sensors and technologies must be encouraged. In that regard, the manuscript does represent a significant contribution towards a better comprehension of the marine methane cycle, and therefore, deserves to be published in OS, upon minor revision. However, I would not say this is a first. Yes it is the first time that this particular technology is deployed in operational conditions – with satisfying results – but this is not the first attempt to get a high-resolution map of CH4 distribution in marine environments. Just to name a few studies on the subject: Sommer et al 2015 (10.1016/j.marpetgeo.2015.08.020), Gentz et al 2014 (10.4319/lom.2012.10.317), Wankel et al 2009 (10.1016/j.dsr2.2010.05.009)... Perhaps, this new sensor has better performance in terms of detection limits and response time, but it's very hard to find them in the manuscript. How does the MILS compare to them?
The development of CH4 sensors has been the holy grail for decades now, and a few technologies emerged from this effort. Each of them were considered as the new solution but I think the main mistake is to believe that one instrument can address the full range of concentrations encountered in the ocean – from 0.1 nM to several mM. This is of course not possible and the instrument must be adapted to the scientific question. In that regard, the MILS seems to be very well adapted to the environmental conditions in which it was deployed. Can the MILS be deployed in oligotrophic waters, i.e. at very low concentrations? And can it measure very high concentrations like in the Black Sea or in the Baltic Sea? One big question at the moment is the role of phytoplankton blooms on the emission of methane to the atmosphere. There are many areas in the open ocean that are characterised by

methane anomalies in the upper layer (i.e. the ocean methane paradox). Concentrations are not necessarily very high (up to 5 nM) but enough to oversaturate the upper layer, and therefore create a positive flux to the atmosphere. Is the MILS able to measure concentrations in this range? I think the effort must be now pointed to low concentration measurements. Anyhow, if one can adapt this instrument to lower concentrations, and then if it can be deployed on AUVs (or any other autonomous platforms), then we will definitely advance the knowledge on the marine CH4 budget. The ideal would be to use this kind of instruments for process studies, i.e. in situ measurements of production/ consumption rates, which will further advance the comprehension of the biogeochemical cycle of methane.

AR: Thank you for taking the time and effort to read and comment on our study. You have acknowledged the importance of this type of investigations. We feel confident that we will see more high-resolution surveys of the same type in the future. In your general comments, you specifically asked for a graphic describing the numerical models, which also reviewer #1 asked for. We added an illustration along with a caption as a part of a new supplementary document.

Regarding the instrument capability and how it compares to other instruments, we refer to the study of Grilli et al. (2018). We would like to avoid an explicit comparison of the MILS to other instruments in this study, and leave that to an impartial instrument comparison study. On page 3, we already mentioned the work of Gentz et al. (2014). Additionally, we now mention the work of Sommer et al. (2015), Wankel et al. (2010), and Boulart et al. (2017) in lines 53–57.

The instrument has a specific range of concentrations as you mention, but for instance, the optical spectrometer can be differently tuned or even replaced to improve its sensitivity or to sample more CH_4 enriched waters. The SubOcean (which we call MILS in our study) was deployed in March 2018 at Lake Kivu, measuring up to 3 mM of CH_4. The report from the Lake Kivu campaign is found here: https://www.dora.lib4ri.ch/eawag/islandora/object/eawag%3A18541/datastream/PDF/Schmid-2019-Intercalibration_campaign_for_gas_concentration-%28published_version%29.pdf.

We believe the MILS would be an excellent tool for evaluating CH4 related water column processes. Grilli et al. (2018) reported a sensitivity of ±25 ppbv in air, translating into ±0.03 nmol l^{-1} at 20 °C and a salinity of 38, which is low enough for investigations of atmospheric exchange and CH4 production/ consumption rates.

MC: We added a graphic (Fig. SI 1) describing the numerical models in the supplementary document.

MC: The works of Sommer et al. (2015), Wankel et al. (2010), and Boulart et al. (2017) are now mentioned in lines 53-57

MC: In lines 408–411, we added a note on the suitability of the MILS for detailed charting of water column processes and ocean-atmosphere interaction.

RC: Specific comments Line 28: I would rephrase 'contributing to minimum oxygen zone formation, and possibly to ocean acidification, as a result of the oxidation of methane'. This last point is still under debate as it is impossible to evaluate precisely the contribution of methane oxidation to the production of CO2 (again because of the lack of in situ data). And yet, the dynamics of these 2 gases are very different.

AR: To our knowledge, the effect of CH_4 oxidation on ocean acidification is today still unknown, and has so far only been modelled. We have rephrased this sentence.

MC: Rephrased sentence in line 27–29.

RC: Lines 40 to 49. I would moderate the discussion here. I think we should view echosounding as a complementary technique to dissolved gas measurements. The big advantage of the echosounding technique is to locate seeping areas while measuring only dissolved methane cannot help deciphering the sources. As for example, in the Black Sea, concentrations are so high that it is impossible to detect the seeping areas other than using echosounding. One advantage I can see is to evaluate the dynamics of bubble dissolution in the water column as gas bubbles are a mean of transfer of methane from the bottom to the surface.

AR: Clearly, the methods described have their own advantages, and one does not exclude the other. We have edited this section and phrased it differently in order to give a more nuanced picture.

MC: Rephrased sentences in lines 40 - 50

RC: Line 53 I would not put in situ mass spectrometry away so quickly. It is commonly used in deep sea studies, especially in hydrothermal environments. Check Boulart et al. 2017, G3. It may have a slower response time but its main advantage is the ability to detect and measure several analytes in the same time.

AR: The MILS is by no means the only solution to in situ measurements of CH_4, and mass spectrometers has the advantage of measuring different dissolved gas species simultaneously. We now mention the Boulart et al. (2017) survey in the text.

MC: The work of Boulart et al. (2017) is mentioned in lines 57–60

RC: Line 101 What is the autonomy of the MILS? What is the power consumption?

AR: 12 h autonomy at 50W.

MC: We now mention the autonomy in lines 99–100.

RC: Line 101 So the MILS uses exactly the same sample introduction system as in situ mass spectrometers. I guess this is the same kind of PDMS membranes? As the authors wrote, membranes are sensitive to fluctuating

water flow. I would add ‘pressure of deployment’ as well. Membrane’s permeability is not the same when deployed at the surface and at 100m depth. How is the pressure effect calibrated? A table comparing MILS’ performance with other instruments would be useful here, so the reader can see the advantages of using MILS rather than an ISMS or something else.

AR: Composite PDMS membranes were used. PDMS permeability is not significantly affected by the water pressure at these depths. (Robb, 1968)

RC: Line 114 What do the authors mean by ‘careful positioning of the SBE5T’? How do they minimize the pressure change? Is the pump very close to the membrane inlet?

AR: The pump was positioned about 25cm away from the membrane inlets and connected with short ½” hose sections and a T piece. By shielding the inlet and outlets and mounting them at the same height with an open flow path pressure changes due to movement through the water column were minimised.

MC: We rephrased the sentences in lines 121–123.

RC: Lines 185-195 Was it obtained with the SBE or with the Anderaa?

AR: The vertical casts (Figure 2a) were obtained with the Seabird SBE CTD and the TS diagrams (Figure 2b, c) were obtained from the towed Anderaa CTD.

MC: This is now mentioned in the text (lines 200 and 208).

RC: Section 3.2 Why do the author use ‘m above seafloor’ as the vertical scale for their casts? This is unusual and can be confusing for the reader. Please use ‘m below sea level’ for all vertical casts.

AR: We agree that it may be a bit unusual to use ‘m above seafloor’ for the vertical scale, but we are specifically investigating seepage from the seafloor and found it natural to describe the flow from its source. This approach enabled us to evaluate the distribution resulting from seepage.

RC: When is the pump started during vertical or horizontal casts? I guess it is a continuous flow?

AR: The water pump (SBE5T) was started at the surface, and ran continuously for the duration of each deployment**.**

RC: Lines 349-356 The authors do not mention the possibility of methanotrophy (microbial oxidation), which is the main control of the vertical distribution of methane in the water column. They can refer to the studies in the Black Sea where concentrations close to the seafloor is up to 12 µmol/l. See Schmale et al 2011, BGS.

AR: Methanotrophic oxidation is an important sink on a larger scales and longer time scales, but is locally insignificant at sites with intense CH_4 bubble seepage and high water through-flow and therefore short residence times (Jansson et al., 2019).

Boulart, C., Briais, A., Chavagnac, V., Révillon, S., Ceuleneer, G., Donval, J.-P., Guyader, V., Barrere, F., Ferreira, N., Hanan, B., Hémond, C., Macleod, S., Maia, M., Maillard, A., Merkuryev, S., Park, S.-H., Ruellan, E., Schohn, A., Watson, S., and Yang, Y.-S.: Contrasted hydrothermal activity along the South-East Indian Ridge (130°E–140°E): From crustal to ultramafic circulation, Geochemistry, Geophysics, Geosystems, 18, 2446-2458, 10.1002/2016GC006683, 2017.
Gentz, T., Damm, E., Schneider von Deimling, J., Mau, S., McGinnis, D. F., and Schlüter, M.: A water column study of methane around gas flares located at the West Spitsbergen continental margin, Continental Shelf Research, 72, 107-118, 10.1016/j.csr.2013.07.013, 2014.
Grilli, R., Triest, J., Chappellaz, J., Calzas, M., Desbois, T., Jansson, P., Guillerm, C., Ferré, B., Lechevallier, L., Ledoux, V., and Romanini, D.: Sub-Ocean: Subsea Dissolved Methane Measurements Using an Embedded Laser Spectrometer Technology, Environmental Science & Technology, 52, 10543-10551, 10.1021/acs.est.7b06171, 2018.
Jansson, P., Ferré, B., Silyakova, A., Dølven, K. O., and Omstedt, A.: A new numerical model for understanding free and dissolved gas progression toward the atmosphere in aquatic methane seepage systems, Limnology and Oceanography: Methods, 0, doi:10.1002/lom3.10307, 2019.
Robb, W.: Thin silicone membranes-their permeation properties and some applications, Annals of the New York Academy of Sciences, 146, 119-137, 1968.
Sommer, S., Schmidt, M., and Linke, P.: Continuous inline mapping of a dissolved methane plume at a blowout site in the Central North Sea UK using a membrane inlet mass spectrometer – Water column stratification impedes immediate methane release into the atmosphere, Marine and Petroleum Geology, 68, 766-775, 10.1016/j.marpetgeo.2015.08.020, 2015.
Wankel, S. D., Joye, S. B., Samarkin, V. A., Shah, S. R., Friederich, G., Melas-Kyriazi, J., and Girguis, P. R.: New constraints on methane fluxes and rates of anaerobic methane oxidation in a Gulf of Mexico brine pool via in situ mass spectrometry, Deep Sea Research Part II: Topical Studies in Oceanography, 57, 2022-2029, 10.1016/j.dsr2.2010.05.009, 2010.

Authors replies to the interactive comments of anonymous referee #3 (11 June 2019) on “High-resolution under-water laser spectrometer sensing provides new insights to methane distribution at an Arctic seepage site” by Pär Jansson et al.

RC: denotes referee’s comments

AR: denotes authors’ reply

MC: denotes manuscript changes

RC: The manuscript by Pär Jansson et al "High-resolution under-water laser spectrometer sensing provides new insights to methane distribution at an Arctic seepage site“ describes the application of a new methane sensor to methane seeps off Svalbard. As the sensor measures methane in situ with a high temporal resolution a very accurate methane inventory of this probably highly variable area is given. Overall the Ms is well written and straightforward. However, the figures contain too much information, which is either not well explained or not necessary for the specific message, and thus are sometimes rather confusing. For a “non-modeller” I found it sometimes difficult to follow the outline of the applied models. In the discussion, both the technical and the scientific aspects should be discussed, But both are rather short. I would be interested in the comparison with the other commercial methane sensor which was attached to the device. . ... Also an estimation on which temporal resolution is really necessary to dissolve the methane distribution would be appreciated, and what influence has the towing speed on the pattern?? More detailed comments can be found in the attached pdf-file

AR: Thank you for taking the time and effort to read and comment on our manuscript. You acknowledge the need for this kind of research, and recognize the hardship of acquiring useful data, even with the new advanced technology. We appreciate your comments, which we believe improved the manuscript.

Regarding your comment that some of the figures contain too much information, Figure 3 has been split into two parts and the information about concentration gradients have been moved to a supplementary section. We also improved the resolution of figure 4. We prefer to keep the “MILS all” in the figure, since it shows the general vertical distribution, which is not shown anywhere else in the manuscript. We put the inset maps in the figure to visualise the origin of the different data points so it would be easier to see the spatial separation between them.

We now supply a visualisation of the model domains in the supplementary information for a better understanding of the control volume and 2D model, as also requested by two other referees.

The technical details of the MILS has been largely omitted in this manuscript, because the instrument has already been thoroughly described in a previous publication (Grilli et al., 2018) . Here, we evaluate its functionality in this particular environment, with a focus is on what we can learn from the high-resolution measurements. This is why the technical discussion is short.

We agree that a comparison with the reference sensor would be interesting. However, for this publication, we decided to refrain from a direct sensor comparison, as we would rather leave it to a non-biased future publication to compare the MILS, the reference sensor and other CH_4 sensors in a more technical publication.

Regarding the resolution, towing speed and the sampling frequency, we believe that we have good enough resolution, since the MILS picks up the concentration gradients along the ship track. See lines 278–280 and the new Fig. SI 2 in the supplementary information. If we want better resolution in three dimensions, we would need denser surveys, and so it will always be a trade-off between costs and data resolution.

Hereafter is a list of comments and suggestions from the referee, which was posted as pop-up notes in a supplement to the comments. Care has been taken to include all comments and suggestions, and answers given to the best of our ability.

RC: Line 99: At which speed was the ship moving ??

AC: The ship's position was logged continuously and can be found in the file in the data repository. During Line 3, the average speed was 0.79 m/s (1.5 knots) with a standard deviation of 0.065 m/s (0.13 knots).

MC: We added a note on the speed on line 105.

RC: Line 101: Can you give an estimate on the accuracy of this distance ??

AC: We added this information on lines 254–255.

RC: Line 151: What is meant with control volume ??

AR: In engineering literature, a control volume is a region fixed in space and its surfaces are called control surfaces. (e.g. Kundu et al., 2008).

MC: We now clarify it on line 164

RC: Line 186: In October 2015, ...

AR: We rephrased this sentence

MC: Line 200 was changed accordingly.

RC: Line 186: I find the two "depth" or "height" definitions confusing, I suggest to use only one of them…

AC: We changed the phrase so it is easier to read, and are now avoiding usage of two different abbreviations.

MC: Lines 200–201 were changed accordingly

RC: Line 222–225: That is too much information in one figure…I suggest to shift the inlet and additional infos on line 3 into an extra figure… The gradient story is not mentioned in the text, thus if rather confusing here…

AR: We followed your advice and split this information into two figures. Figure 3 now focuses only on the concentrations along the five main trajectories. The caption has been truncated accordingly. A new figure, visualising the gradients, is included in the supplementary document (Figure SI 2). The gradients are discussed on lines 272–283.

MC: New figure 3. Caption of figure 3 truncated. New figure in supplementary document (Fig. SI 2).

RC: Line 226–229 : This technical information should go either M&M or

AR: We now describe this in the methods section, and mention the results in the appropriate section.

MC: Lines 139–141 and lines 236–238

RC: Line 230: Again, there is too much information in the figure 4, which is then not mentioned in the text... please refrain to the important facts. If you only want to compare the vertical casts of CTD 616, 618,619 than all other informations are not needed and are more confusing....

AR: We believe that visualising the different measurements together with their spatial separation is key to understanding the heterogeneity of the CH_4 distribution. It may take some effort to appreciate this figure, but we think it is valuable to show the spatial separation together with the concentration data, in order to realise the distribution of dissolved CH_4.

RC: Line 247: But there are also areas with strong bubble streams but with low methane concentrations ?? For example at the very left side of the figure ??

AR: From our experience with echosounder data, no bubble streams are visible in the echogram on the left side of the figure. Conversely, there are methane peaks without visible flares, which we discuss at some length on lines 374–385. On the right hand side of the figure, there are flares without increased concentrations. This may be due to the fact, that the echosounder swath width is ~40 m at the seabed, while the MILS measures locally. Therefore, it is possible that we passed nearby a flare, which was acoustically identified but that we were too far away to see the CH_4 plume in the MILS data.

RC: Line 249: Again too much information here: what for are the upper inserts needed? And MILS all ?? What about the other DS from the casts along line 3, 1623, 1621, ff ??

AR: See our comment above about line 230. Comparison between the discrete samples from CTDs, and MILS data from line 3 data can be seen in Figure 7, which has been improved also after the request from another referee.

MC: Figure 7 has been improved

RC: Line 250: remove from figure and legend

AR: See our answer regarding line 230 and 249. We believe that this visualisation helps to understand the vertical distribution.

RC: Line 255–259: remove from figure and legend, I think it is sufficient to mention that the CTD casts were xx m away.

AR: See our answer regarding line 230 above.

RC: Line 262: The blue line is hardly visible, but propably also not necessary as already shown in figure 1.

AR: The blue line does not stand out very well in this document, but it looks good in the original figure. We think it will be clear in the final version without any changes. The instrument position is shown in Figure 1, but the depth is not indicated. The depth is shown in Figure 3, but has no reference. In this figure, it is presented to scale with the echosounder data, which we believe is important for the interpretation.

RC: Line 265: I do not understand what is meant with upstream and downstream gradient, and thus also can not follow your conclusions…

AC: We have removed the gradients from figure 3 and moved this information to the supplementary information. In the new figure (SI 2), the upstream/ downstream gradients are explained and visualised. Thanks for directing our attention to this. It was not very clear earlier.

MC: New Fig. 3 and new Fig. SI 2.

RC: Line 268–276: ???? I can not follow here and I am not sure if this information on the instrument characteristics is necessary here, as this should have been done in the previous publication and not its application now…

AR: Here we argue that the instrument has good enough resolution for this particular environment. It is not about the technical aspects of the instrument itself, but that we managed to resolve the CH_4 distribution by towing the probe with the right settings at the right speed, so it could pick up the heterogeneity.

RC: Line 292: could you indicate the stream / current in the figure ?

AR: Yes, of course.

MC: We added an arrow in this figure and in Figure SI 2.

RC: Line 297: But also the water depth of the instrument was more stable in this area, compared to the fluctuation before and after…

AR: After double-checking the data, we found that the relative standard deviations of the probe depth, salinity, and temperature is lower by factors of 3, 10, and 58, when compared to the upstream (later in time) data. This is consistent with the notion that the "flat profiles" between 10:50 and 11:15 are caused by enhanced turbulent mixing due to bubble streams. The standard deviation of the probe depth dropped by a factor of 3 which is not enough to explain the larger drops in salinity and temperature standard deviations. It is normal that temperature diffuses faster than salinity (see textbooks on ocean turbulence), so the fact that the temperature profile is flatter than the salinity profile has a reasonable explanation. We re-phrased the sentence to describe this feature more accurately. Thanks for noticing that.

MC: Lines 305 – 309

RC: Line 302: but is it a good match ?? the methane peaks on the left side are not resolved in the modell and at the right side the model seems to be shifted…

AR: We are not arguing that this is a good match. It is simply the best of the performed simulations, which are solely based on flare observations and the assumptions of a homogenous, steady water current along the domain, homogenous and constant diffusion etc. We do not expect a perfect match from such a simple model, but find it striking that the model does so well with so little information. The lack of sources for the downstream (left) peaks are mentioned in the discussion. We do not have an immediate explanation for the apparent shift on the right hand side of the figure. It could be due to undiscovered sources, imperfect time lag correction of the instrument data, wrong assumption of homogenous water current or it can be explained by the relatively large swath of the echosounder while the MILS measure locally (see our reply to the RC comment about line 247).

RC: Line 326: I find it difficult to understand how you calculated the average concentration of the specific area and being a non-modeller, when you compare a average shouldn't there be a standard deviation ?? To judge if 47 is about the same as 77 nM. ??

AR: The model domain is now visualised in the supplementary information and the improved Figure 7 shows the discrete and high-resolution data, which underlies the average calculations. The caption for Table 1 explains how the data was averaged. The point is that high-resolution data makes a better estimate for a CH_4 inventory, while sparse sampling can easily over- or underestimate the inventory. Standard deviation does not make sense here, but one should keep in mind the uncertainties of the methods (4% for the discrete samples and 12% for the MILS data). The model builds on "flare quantification" with uncertainties related to bubble sizes and rising speeds, discussed at length in Veloso et al. (2015). The model has a correlation with the high-resolution data of 0.68, so should be evaluated with care.

RC: Line 353: but still below the pycnocline ... aha.. this was well below the pyccnocline, thus background levels of methane were reached below the pycnocline, which there fore could not act as barrier... Maybe you should re-phrase your argumentation here...

AR: That would be a way of saying the same thing, but it does not help to understand the mechanism. We believe it is appropriate to give a plausible explanation, rather than just stating the obvious fact that vertical transport is inefficient. Here we explain why it is not necessary to have a pycnocline to impede vertical transport of solvents (in this case dissolved CH_4). A small continuous stratification is enough. The argument that wintertime stratification-breakdown can cause sudden emissions of CH_4 to the atmosphere still stands.

Grilli, R., Triest, J., Chappellaz, J., Calzas, M., Desbois, T., Jansson, P., Guillerm, C., Ferré, B., Lechevallier, L., Ledoux, V., and Romanini, D.: Sub-Ocean: Subsea Dissolved Methane Measurements Using an Embedded Laser Spectrometer Technology, Environmental Science & Technology, 52, 10543-10551, 10.1021/acs.est.7b06171, 2018.

Veloso, M., Greinert, J., Mienert, J., and De Batist, M.: A new methodology for quantifying bubble flow rates in deep water using splitbeam echosounders: Examples from the Arctic offshore NW-Svalbard, Limnology and Oceanography: Methods, 13, 267-287, 10.1002/lom3.10024, 2015.

High-resolution under-water laser spectrometer sensing provides new insights to methane distribution at an Arctic seepage site

Pär Jansson[1], Jack Triest[2], Roberto Grilli[2], Bénédicte Ferré[1], Anna Silyakova[1], Jürgen Mienert[1], Jérôme Chappellaz[2]

[1] CAGE Center for Arctic Gas Hydrate, Environment, and Climate, Department of Geosciences, UiT-The Arctic University of Norway, 9037, Tromsø, Norway
[2] Univ. Grenoble Alpes, CNRS, IRD, Grenoble INP, IGE, 38000 Grenoble, France

Correspondence to: Pär Jansson (per.g.jansson@uit.no), Roberto Grilli (roberto.grilli@cnrs.fr)

Abstract. Methane (CH_4) in marine sediments has the potential to contribute to changes in the ocean- and climate system. Physical and biochemical processes that are difficult to quantify with current standard methods such as acoustic surveys and discrete sampling govern the distribution of dissolved CH_4 in oceans and lakes. Detailed observations of aquatic CH_4 concentrations are required for a better understanding of CH_4 dynamics in the water column, how it can affect lake- and ocean acidification, the chemosynthetic ecosystem, and mixing ratios of atmospheric climate gases. Here we present pioneering high-resolution in-situ measurements of dissolved CH_4 throughout the water column over a 400 m deep CH_4 seepage area at the continental slope west of Svalbard. A new fast-response under-water membrane-inlet laser spectrometer sensor demonstrates technological advances and breakthroughs for ocean measurements. We reveal decametre-scale variations of dissolved CH_4 concentrations over the CH_4 seepage zone. Previous studies could not resolve such heterogeneity in the area, assumed smoother distribution and therefore lacked both details and insights to ongoing processes. We show good repeatability of the instrument measurements, which are also in agreement with discrete sampling. New numerical models, based on acoustically evidenced free gas emissions from the seafloor, support the observed heterogeneity and CH_4 inventory. We identified sources of CH_4, undetectable with echosounder, and rapid diffusion of dissolved CH_4 away from the sources. Results from the continuous ocean laser-spectrometer measurements, supported by modelling, improve our understanding of CH_4 fluxes and related physical processes over Arctic CH_4 degassing regions.

1 Introduction

Methane (CH_4) release from gas bearing ocean sediments has been of high interest for many years (e.g. ~~Jørgensen et al., 1990;~~ Westbrook et al., 2009;~~-~~Ferré et al., 2012;~~-~~Ruppel and Kessler, 2016;Jørgensen et al., 1990;Boetius and Wenzhöfer, 2013; Myhre et al., 2016;~~ Ruppel and Kessler, 2016;~~ Platt et al., 2018). Once released and dissolved in the water column, the CH_4 gas diffuses and is partly oxidized in the water column (Reeburgh, 2007), contributing to minimum oxygen zones (Boetius and Wenzhöfer, 2013) and possibly to ocean acidification (Biastoch et al., 2011)~~ and minimum oxygen zone formation (Boetius and Wenzhöfer, 2013).~~. Chemosynthetic life on the seabed depends on the supply of methane as an energy resource (e.g. Boetius and Wenzhöfer, 2013). Supply of nutrient rich bottom water, by means of local upwelling, may enhance biological productivity, induce drawdown of CO_2 from the atmosphere, potentially making shallow CH_4 seepage sites sinks for this critical greenhouse gas (Pohlman et al., 2017). Warming of ocean bottom waters, active tectonics and ice sheet build up and retreat could, at different time scales, lead to CH_4 gas release from the seabed ~~(e.g. Portnov et al., 2016)~~(e.g. Portnov et al., 2016). The magnitude and trend of such a phenomena are still under debate (e.g. Hong et al., 2018;Ruppel and Kessler, 2016; Andreassen et al., 2017~~; Hong et al., 2018~~) and accurate methods to measure methane concentration from its source are needed. At shallow seepage sites, such as the East Siberian Arctic Shelf, CH_4 can potentially reach the atmosphere and amplify greenhouse warming (Shakhova et al., 2010;-Shakhova et al., 2014). However, most studies of shallow CH_4 seepage sites have

found no or little CH_4 flux to the atmosphere (e.g. ~~Gentz et al., 2014; Myhre et al., 2016;~~ Miller et al., 2017;~~-~~Platt et al., 2018;Myhre et al., 2016;Gentz et al., 2014).

In the past, most CH_4 measurements relied on indirect or discrete sample measurements (e.g. Damm et al., 2005;~~-~~Westbrook et al., 2009;~~-~~Gentz et al., 2014). Bubble catcher and mapping with multibeam echosounder (Sahling et al., 2014), hydro-acoustic imaging together with bubble size and bubble rising speed measurements (~~Ostrovsky, 2003; Greinert et al., 2006;~~ Sahling et al., 2014;~~-~~Weber et al., 2014;~~-~~Veloso et al., 2015;Greinert et al., 2006;Ostrovsky, 2003) have been used to derive CH_4 flow rates. The acoustic ~~indirect~~ method ~~can only quantify~~effectively maps CH_4 ~~fluxes~~seepage from acoustically detectable ~~bubbles~~sources, and ~~ROV's can only capture visible bubbles, while neither can~~camera equipped ROVs can investigate their properties. However, these methods cannot detect CH_4 from sources other than free gas seepage~~. These methods~~ and do not provide information about the distribution of dissolved CH_4 ~~in the water column.~~. Discrete ~~water~~ sampling with Niskin bottles ~~only~~ allows ~~measurement~~3D mapping of ~~the~~ dissolved CH_4 ~~at~~, but is limited ~~spatial~~ by its labour intense nature, with resulting low resolution, ~~and the low horizontal and vertical resolution~~which in turn may lead to ~~artificial~~ smoothing ~~of the spatial distribution~~ and inaccurate ~~estimate~~estimates of ~~average dissolved~~ CH_4 ~~concentration. The method using the~~inventories. The combination of bubble catcher and multibeam echosounder ~~introduces large~~is very efficient once the bubble seepage has been properly categorised, but uncertainties arise while extrapolating ~~CH_4 flow rates from few~~ bubble catcher ~~measurements and applying those~~ flow rates to acoustically evidenced bubble streams (flares). Present commercial underwater CH_4 sensors do not have the required response time for accurate high-resolution mapping. For this reason, Gentz et al. (2014) deployed an underwater membrane inlet mass spectrometer (UWMS) with a fast response time for mapping of CH_4 at shallow (10 m) depths. Boulart et al. (2013) used an in-situ, real time sensor in the Baltic Sea~~, but it was not deployed over a CH_4 seepage site. Furthermore, their reported instrument response time of 1–2 minutes and the detection limit of 3 nmol l^{-1} represent limitations for fast profiling and background concentration studies linked to the atmospheric CH_4 mixing ratio.~~ The instrument response time of 1–2 minutes and detection limit of 3 nmol l^{-1} represent limitations for fast profiling and near surface concentration studies linked to atmospheric exchange. Sommer et al. (2015) used a pump-fed membrane inlet mass spectrometry installation at a blowout location in the North Sea. They achieved a response time of 30 minutes and a detection limit of 20 nmol l^{-1}. Wankel et al. (2010), deployed a deep-sea graded in-situ mass spectrometer over a brine pool in the gulf of Mexico, where they measured high (µM – mM) concentrations of CH_4. They do not specify their detection limit or the response time of the instrument, but state an uncertainty of 11%. Boulart et al. (2017) mapped hydrothermal activity while deploying an in-situ mass spectrometer (ISMS) over the southeast Indian Ridge. The ISMS has the advantage of measuring several dissolved gases simultaneously, but only CH_4 was reported because of the high detection limit of H_2. The ISMS response time and detection limits were not specified.

Here we present the first in-situ, high-resolution ocean laser spectroscopy mapping of dissolved CH_4 in seawater over active CH_4 seepage in the Arctic. The data was collected by deploying a patent based (Triest et al. patent France No. 17 50063)

membrane inlet laser spectrometer (MILS) (Grilli et al., 2018). The high-resolution measurements, together with echosounder data, discrete water sampling, and newly developed control volume and 2-dimensional (2D) models improve our understanding of CH_4 fluxes from the seabed into oceans and lakes, and potentially to the atmosphere.

2 Materials and methods

2.1 Study area

The survey was performed on board ~~R/V~~RV Helmer Hanssen, UiT, The Arctic University of Norway, in October 2015 (CAGE 15-6 cruise) west of Prins Karls Forland located offshore western Svalbard. Over a period of three days (October 21–23), we surveyed an area of ~18 km^2 at water depths between 350 and 420 m, using continuous under-water laser spectroscopy as well as traditional discrete sampling for dissolved CH_4, and echosounding for bubble detection and gas seepage quantification. The study area is located at 78°33´ N, 9°30´ E over an active CH_4 venting area (Fig. 1a). Here, more than 250 flares (acoustic signature of bubble streams in echograms) exist along the shelf break (e.g. ~~Damm~~Sahling et al., ~~2005;~~ 2014;Westbrook et al., 2009; ~~Berndt~~Damm et al., ~~2014; Sahling et al., 2014;~~ 2005;Graves et al., 2015;Berndt et al., 2014). The northward flowing West Spitsbergen Current (WSC), which transports Atlantic Water (AW, S>34.9, T>3° C) (Schauer et al., 2004), controls the hydrography of the study area. The East Spitsbergen Current (ESC), flows south-westward along the eastern Spitsbergen coast, and northward along the western Svalbard margin, carrying Arctic Surface Water (ASW, $34.4 \leqslant S \leqslant 34.9$) and Polar Water (PW, S<34.4) (Skogseth et al., 2005). The Coastal Current (CC), extension of the ESC (Loeng, 1991; Skogseth et al., 2005), contributes a transient addition of ASW and PW on the shelf and the continental slope as the WSC meanders on- and offshore ~~(Steinle et al., 2015).~~(Steinle et al., 2015). The Lower Arctic Intermediate Water (LAIW, S>34.9~~‰~~, $T \leqslant 3$ °C) flows below the Atlantic Water (Ślubowska-Woldengen et al., 2007).

2.2 Hydrocasts with discrete water sampling

Vertical oceanographic profiles were recorded at 10 stations (Fig. 1a) using a Seabird SBE 911 plus CTD (Conductivity, Temperature, and Depth) mounted on a rosette, which carried twelve 5-liter Niskin bottles. In January 2015, the CTD was fitted with new sensors~~; an~~. An SBE 4 Conductivity Sensor and an SBE 3plus Premium CTD Temperature Sensor, with initial accuracies of ± 0.001 °C and ± 0.~~0003 S~~3 mS m^{-1}. At 24 Hz sampling, the resolutions are 0.0003 °C and 0.~~00004 S~~04 mS m^{-1}.

The Niskin bottles were closed during the up-casts, collecting seawater at different depths for further dissolved CH_4 analysis. Headspace equilibration followed by gas chromatography (GC) analysis was carried out in the laboratory at the Department of Geoscience at UiT, The Arctic University of Norway, using the same technique as Grilli et al. (2018). The resulting headspace mixing ratios (ppmv) were converted to in-situ concentrations (nmol l^{-1}), using Henry's solubility law, with coefficients calculated accordingly with Wiesenburg and Guinasso (1979). The sample dilution from addition of a reaction stopper (1 ml of 1M NaOH solution replacing 1 ml of each 120 ml sample), and the removal of sample water while introducing

headspace gas (5 ml of pure N_2 replacing 5 ml of sample water) was accounted for. The overall error for the headspace GC method was 4%, based on standard deviation of replicates.

2.3 Methodology and technology for high-resolution laser spectrometer CH_4 sensing

A stainless steel frame attached to a cable ~~that was~~ connected to an on-board winch served as a platform to which the MILS, an Aanderaa, Seaguard TD262a CTD, a standard commercial CH_4 sensor, and a battery pack were mounted. This instrument assembly, hereafter called ~~the~~ "probe~~,~~", has a total height of ~1.8 m, a total weight in air of ~160 kg and a negative buoyancy of ~52 kg. We towed the probe for a total of 28 hours, providing unsurpassed high-resolution in-situ CH_4 measurements with a sampling rate of 1 s^{-1}, together with dissolved oxygen data, as well as pressure, temperature and salinity. The autonomy of the MILS was ~12 hours at 50 W power consumption. The sensors fitted to the Aanderaa CTD, a Conductivity Sensor 4319, a Temperature Sensor 4060, and an Oxygen Optode 4330, has initial accuracies of ± 0.~~005 S~~03°C , ± 5 mS m^{-1}, ~~± 0.03°C,~~ and < ± 8 µM and ~~the~~ resolutions ~~are 0.0002 S m^{-1}~~ ,of 0.001 °C, 0.2 mS m^{-1}, and < 1 µM, respectively.

Lowering and heaving of the probe in the water column allowed for vertical casts, while towing the probe behind the moving ship at varying heights above the seafloor generated near-horizontal trajectories. The main horizontal trajectories, acquired at a ship speed of 1.5 ± 0.15 knots, comprise five lines (Fig. 1a), where the desired distance ~~(~15 m)~~ from the seafloor was attained by monitoring the pressure in real time while adjusting the cable payout. The battery-powered MILS (Fig. 1b, see Grilli et al. (2018) for more details) has a membrane inlet system, linked to an optical feedback cavity-enhanced absorption spectrometer and an integrated PC for control and data storage. Cabled real-time communication with the instruments allowed instant decision-making, and ensuring optimal sensor operation during the deployments.

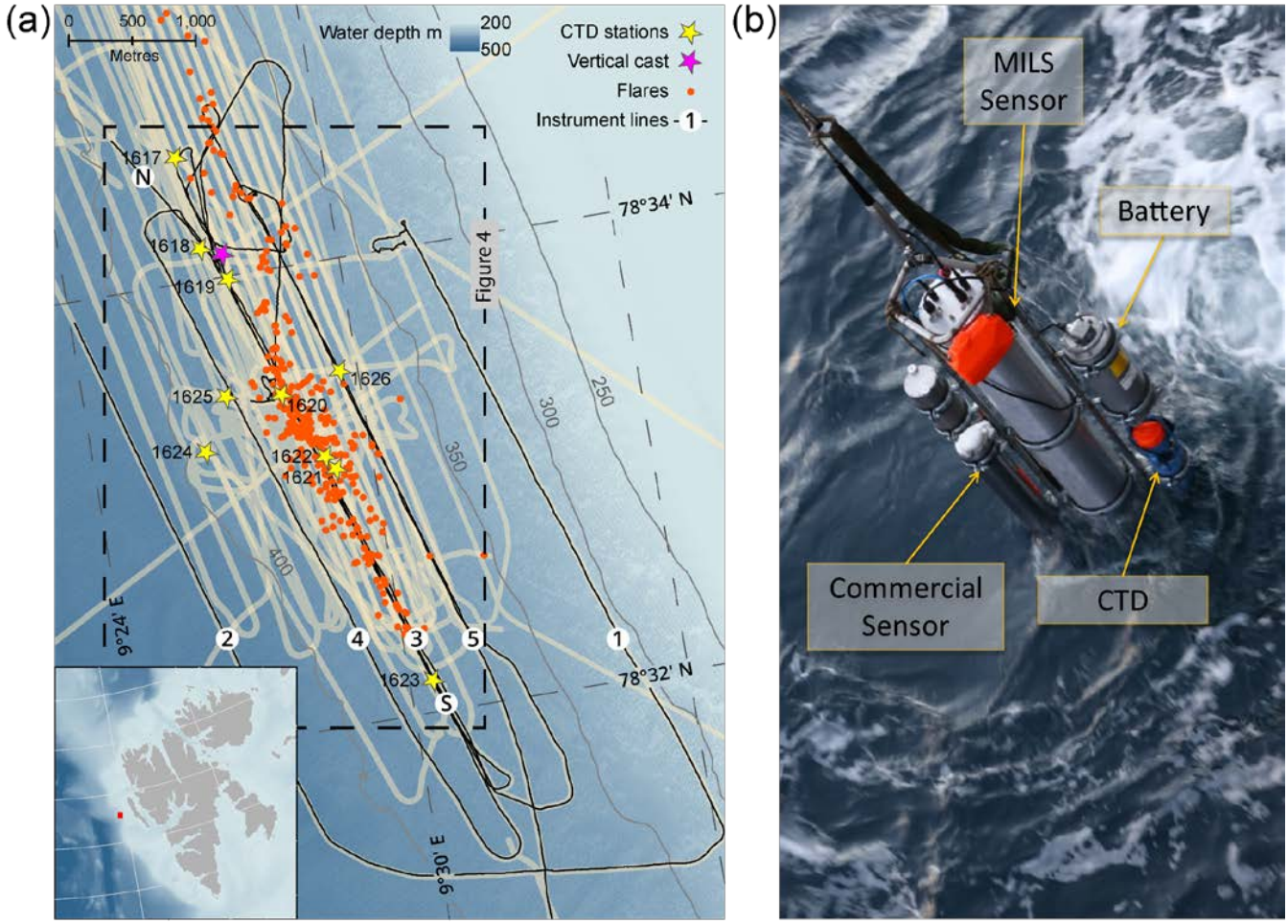
(a)
0
500
1,000
Metres
Water depth m
200
500
CTD stations
Vertical cast
Flares
Instrument lines - 1 -
1617
N
1618
1619
1625
1626
1620
1624
1622
1621
1623
S
Figure 4
78°34' N
78°32' N
9°24' E
9°30' E
250
300
350
400
1
2
3
4
5
(b)
MILS Sensor
Battery
Commercial Sensor
CTD

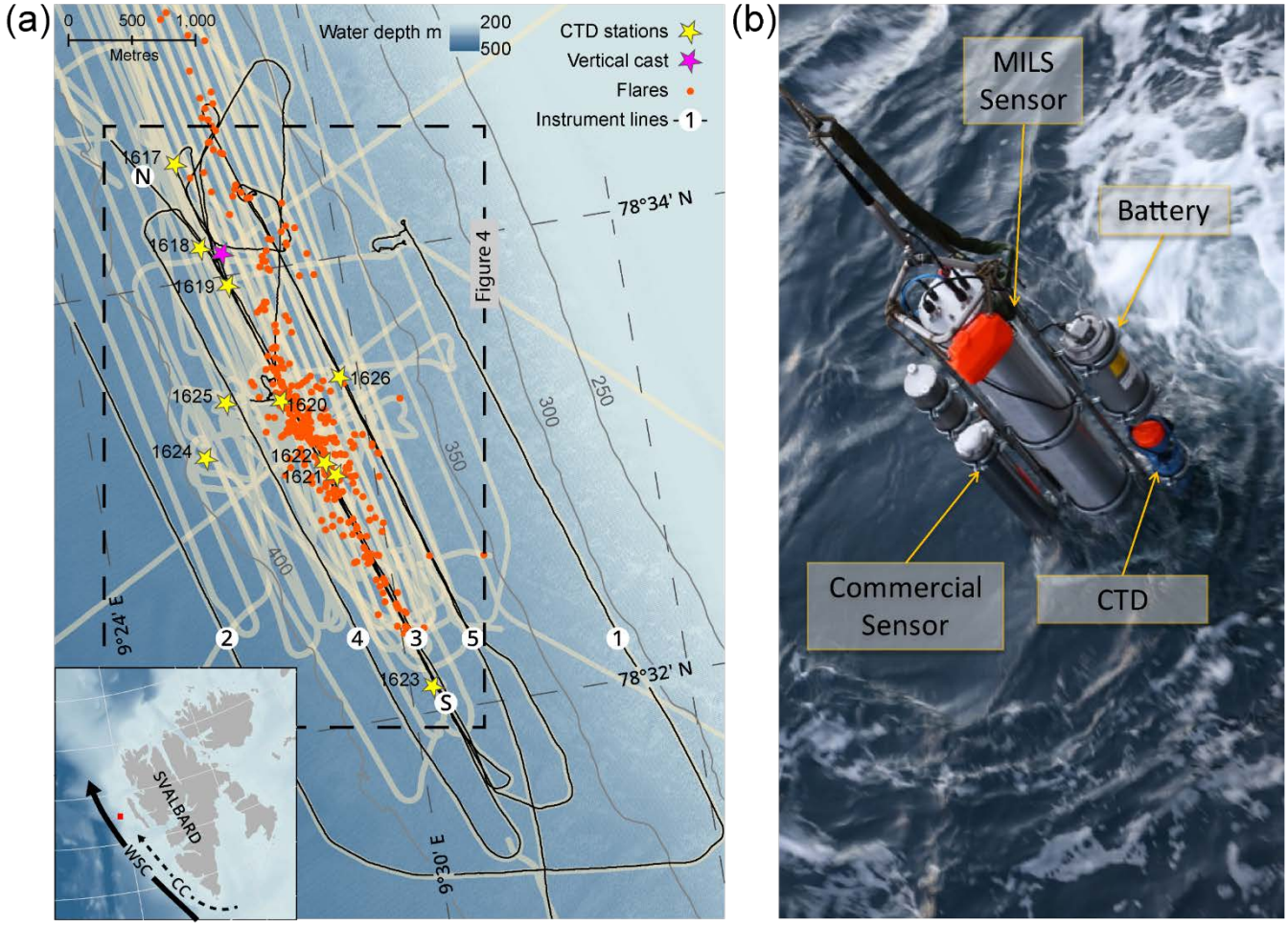

Figure 1: Map of the surveyed area and photo of the instrument assembly. a) Survey lines and sampling locations over the study area at the Svalbard continental margin. Black lines show the ship trajectory with line numbers assigned in the order they were surveyed. Beige areas appearing as thick lines indicate echosounder beam coverage from this campaign and previous cruises (AOEM 2010, and CAGE 13-7 in 2013). The start- and end- locations of line 3 are indicated with N and S respectively. Known flare locations from this survey and surveys in 2010 and 2013 are marked with orange dots. CTD stations with discrete water sampling are marked with yellow stars and the vertical instrument cast with a purple star. The inset image shows an overview of Svalbard with the survey location indicated with a red square. The controlling currents are shown with solid (WSC) and dashed (Coastal current) black lines. b) Instrument assembly. The main central tube is the prototype MILS sensor. The stainless steel frame acts as a platform and allows attachment of instrument battery (top right side), CTD (blue at the bottom right) and a commercial CH_4 sensor and its battery pack (left side).

Sensors with membrane inlets can be sensitive to fluctuating water flow over the membrane, which can result in artificial variability of measured concentrations. ~~Careful positioning of the Sea-Bird SBE5T water pump to minimize inlet, and outlet pressure changes and subsequent flow variations minimized this effect.~~The SBE5T pump was positioned about 25cm away from the membrane inlets and connected with short ½" hose sections and a T piece. By shielding the inlet and outlets and mounting them at the same height with an open flow-path, pressure changes due to movement through the water column were minimised. The water pump inlet has a fine mesh filter and a shield to avoid entry of free gas bubbles and artefacts from gas bubbles entering the sampling unit and reaching the membrane surface.

All parameters from the MILS sensor, including gas flow, pressure, sample humidity, and internal temperature were logged to process and evaluate the quality of the data. A dedicated ship-mounted GPS logged positional data for accurate synchronization

of the probe and ship position. A position correction, accounting for the lag between the probe and the ship synchronizes the towed instrument data with simultaneously acquired echosounder data. The Matlab routine "Mooring Design and Dynamics" (Dewey, 1999) simulated the towing scenario, for which we used a simplified instrument assembly composed by a cylinder 1.68 m long, 0.28 m diameter with a negative buoyancy of 52 kg~~.~~, corresponding to the volume and buoyancy of the whole instrument assembly. A polynomial speed-factor ($x_* = -0.2211u^5 + 1.355u^4 - 3.0126u^3 + 2.6741u^2 - 0.1609u$) was derived to account for the combined ship- and water current velocities (u in m s^{-1}). The distance of the probe behind the ship and the corresponding required time-shift was calculated by multiplying the non-dimensional speed-factor~~-~~(x_*) with the instrument depth at each data point. This approach allowed for dynamic correction of data positions, accounting for towing with or against the water current and a near-stationary ship during vertical profiling. Correction for tidal currents was neglected since tides constituted less than 5% of the WSC of ~0.2 m s^{-1} during our deployments, according to the tide model TPXO (Egbert and Erofeeva, 2002).

A time lag of 15 sec for the MILS was calculated based on the volume of the gas line between the extraction system and the measurement cell and the gas flow rate. We expect that concentrations profiles obtained from down- and up-casts align when this time lag is applied. The response time of the MILS is given by the flushing time of the measurement cell, and for this campaign, the T_{90} was 15 sec.

Mixing ratios of CH_4 (ppmv) measured by the MILS were converted into aqueous concentrations (nmol l^{-1}) using Henry's law, where the solubility coefficients were determined accordingly with Wiesenburg and Guinasso (1979), while accounting for in-situ pressure, temperature, and salinity. The uncertainty of the dissolved CH_4, measured with the MILS is ± 12% (Grilli et al., 2018).

2.4 Acoustic mapping and quantification of seafloor CH_4 emissions

Gas bubbles in the water column are efficient sound scatterers and ship-mounted echosounders can therefore be used for identifying and quantifying gas emissions (~~Ostrovsky et al., 2008;~~ Weber et al., 2014;~~-~~Veloso et al., 2015;Ostrovsky et al., 2008). The target strength (TS), defined as 10 times the 10-base logarithmic measurements of the frequency dependent acoustic cross sections (Medwin and Clay, 1997), quantifies the existence of sound scattering objects in the water column. Time series of TS are displayed in so-called echograms (Greinert et al., 2006;~~-~~Judd and Hovland, 2009). During the cruise, the 38 kHz channel of the ship-mounted single beam Simrad EK-60 echosounder recorded acoustic backscatter continuously. Flares can be identified in the echograms and distinguished from other acoustic scatter from fish schools, dense plankton aggregations, and strong water density gradients. We identify flares as features in echograms, which exceed the background backscatter ~~(TS)~~ by more than 10 dB, with a vertical extension larger than their horizontal, and which are attached to the seafloor.

We used the methodology developed and corrected by ~~Veloso et al. (2019)~~Veloso et al. (2015);Veloso et al. (2019a) and the prescribed FlareHunter software for mapping and quantifying gas release. For the flow rate calculations performed with the Flare Flow Module of FlareHunter, we used ~~the~~a bubble size spectra with a Gaussian distribution peaking at 3 mm equivalent

radius, previously observed in the area (Veloso et al., 2015). Temperature, salinity, pressure, and sound velocities, all required for correct quantification, were provided by the CTD casts. The resulting flow rates and seepage positions allow for mass balance calculation in the control volume model and in the two-dimensional (2D) model, as described in Sect. 2.5 and 2.6, respectively.

2.5 Control volume model

The temporal evolution (dC/dt) of a solute's concentration C within a certain volume V, which is fixed in space, and with water flowing through it can, using mass conservation, be written as:

$$\frac{dC}{dt} = \frac{Q_{IN} \times C_B}{V} - \frac{Q_{OUT} \times C}{V} + \frac{F}{V} + k\nabla^2 C \quad (1)$$

Equation (1) is a second order differential equation, from which an analytical steady state solution can be derived by following these assumptions: The volumetric flow of water in and out of the control volume, Q_{IN} and Q_{OUT} are balanced and are given by a steady water current in the x-direction across the width (Δy) and height (Δz) of the control volume. The diffusion is kept homogenous and constant by applying a constant diffusion coefficient k. The background concentration C_B is fixed in time and space and F represents the persistent flow of the solute (in this case bubble mediated CH_4) into the volume. The CH_4 dissolves completely within the volume, and the diffusion occurs across the domain (in the y-direction). Using the central difference approximation of the second derivative (∇^2 in Eq. (1) and the above assumptions yield that the aqueous CH_4 within the volume reaches the steady state concentration:

$$C_{t=\infty} = \left(\frac{Q_{IN} \times C_B}{V} + \frac{F}{V} + \frac{2k \times C_B}{(\Delta y)^2}\right) \times \left(\frac{Q_{OUT}}{V} + \frac{2k}{(\Delta y)^2}\right)^{-1} \quad (2)$$

Finally, by averaging measured CH_4 concentration within a defined volume, and assuming that it represents a steady state concentration, the bubble flow rate is retrieved from Eq. (2).

$$F = (\bar{C} - C_B) \times \left(Q + \frac{V \times 2k}{(\Delta y)^2}\right) \quad (3)$$

Where $\bar{C}$ represents the measured average concentration, and $Q = Q_{IN} = Q_{OUT}$.

The dimensions of the control volume with volume V = $\Delta x \times \Delta y \times \Delta z$, were chosen to match the length of line 3 (Δx = 4.5 km), extended 25 m perpendicularly on each side of the line (Δy = 50 m), and 75 m vertically (Δz = 75 m). A graphic describing the control volume is supplied in Fig. SI 1.

2.6 Two-dimensional model

In order to gain insight to the physical processes behind the observed CH_4 variability, we constructed a two-dimensional (2D) numerical model, resolving the evolution of dissolved CH_4 in the water column, which results from CH_4-bubble emissions, advection with water currents and diffusion. The model domain was made 400 m high in the z-direction, 4.5 km long in the x-direction, and oriented along line 3 (Fig. 1a). The navigation data along this line is linearly interpolated to form the basis for a 2-metre gridded model domain starting at 78°34.~~54'N~~54' N, 9°25.~~92'E~~92' E and ending at 78°32.1' N, 9°30.58' E as indicated

by N and S, in Fig. 1a. FlareHunter derived flow rates within 50 m from line 3 were projected into the model domain, and the source of dissolved CH_4, mediated by bubbles, was distributed vertically by applying a non-dimensional source-function similar to the approach of Jansson et al. (2019): $S0(z) = 6.6 \times 10^{-2} \times e^{-0.066 \times z}$, where z is the vertical distance from the seafloor in metres. We calculated source distribution functions *S(z)* by scaling *S0(z)* with the flare flow rates, and distributed the resulting source into current-corrected x/z nodes with volumes $\delta V = \delta x \times \delta y \times \delta z$, where δx=δy=δz=2 m. The model domain comprises 12 extra cells on each side in the y-direction in order to avoid fast diffusion out of the domain while the background concentration is held constant. The 2D model simulated CH_4 diffusion and advection with water currents, and was run to steady state using different diffusion coefficients, within the range suggested by Sundermeyer and Ledwell (2001). A graphic representation of the 2D model is shown in Fig. SI 1.

3 Results

3.1 Water properties

The ~~water is~~measurements from the Seabird CTD during our survey indicates well-~~-~~mixed water within 150 ~~masf (~~metres above the seafloor~~),~~ and continuously stratified ~~from 250~~water upwards to 50 ~~mbsl (~~metres below the sea level (mbsl) (Fig. 2a) with a squared buoyancy frequency of ~$N^2 < 4 \times 10^{-5}$ s^{-2}. A pycnocline exists at ~30 mbsl (Fig. 2a) with N^2 up to 10^{-4} s^{-2}, marking the transition between surface water and AW below (Fig. 2b and 2c). Temperatures close to the seafloor range from 4.2–4.4 °C, which is more than 1 °C above the CH_4 hydrate stability limit (Tishchenko et al., 2005), for a salinity of 35.1 as indicated in Fig. 2a. The velocity of the WSC was between 0.1 and 0.3 m s^{-1} (Fig. 2d) inferred from the inclination of flare spines (Veloso et al., 2015), ~~and~~which was calculated from the echosounder data, obtained throughout the whole survey. The current followed the isobaths, which is consistent with previous findings (~~Gentz et al., 2014;~~ Graves et al., 2015;Gentz et al., 2014). The mean salinity and temperature~~,~~ acquired with the Andreaa CTD, in different layers, with their corresponding standard deviations according to the water masses classification of Skogseth et al. (2005) and Ślubowska-Woldengen et al. (2007) are shown in Fig. 2b,c. The temperature/ salinity distribution suggests a clear dominance of AW during the survey, overlaid with fresher and colder ASW and PW.

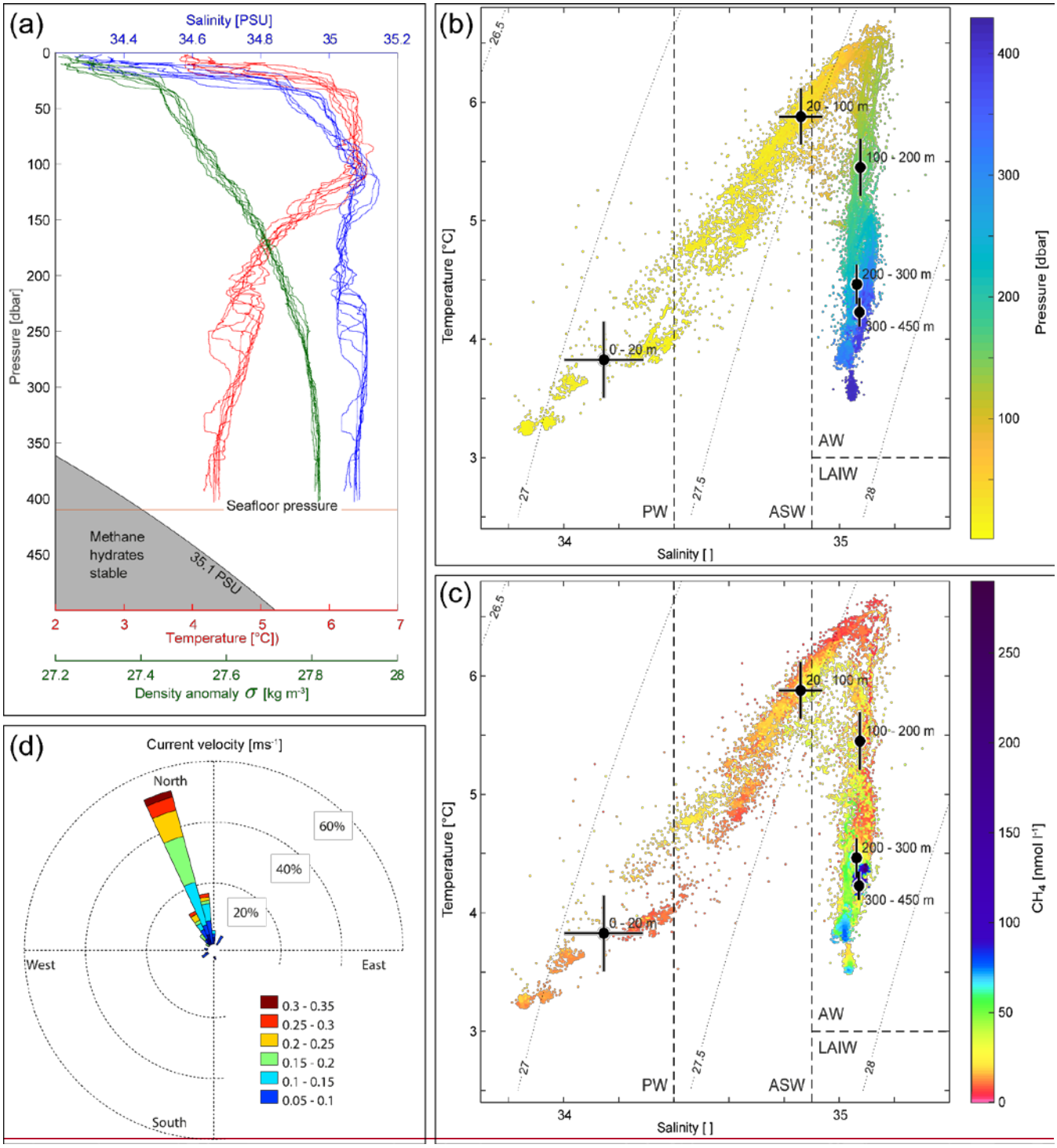
(a)
Salinity [PSU]
34.4
34.6
34.8
35
35.2
Pressure [dbar]
Seafloor pressure
Methane hydrates stable
35.1 PSU
Temperature [°C])
Density anomaly σ [kg m-3]
(b)
Temperature [°C]
Salinity [ ]
0 - 20 m
20 - 100 m
100 - 200 m
200 - 300 m
300 - 450 m
PW
ASW
AW
LAIW
Pressure [dbar]
(c)
CH4 [nmol l-1]
(d)
Current velocity [ms-1]
North
South
West
East
60%
40%
20%
0.3 - 0.35
0.25 - 0.3
0.2 - 0.25
0.15 - 0.2
0.1 - 0.15
0.05 - 0.1

225

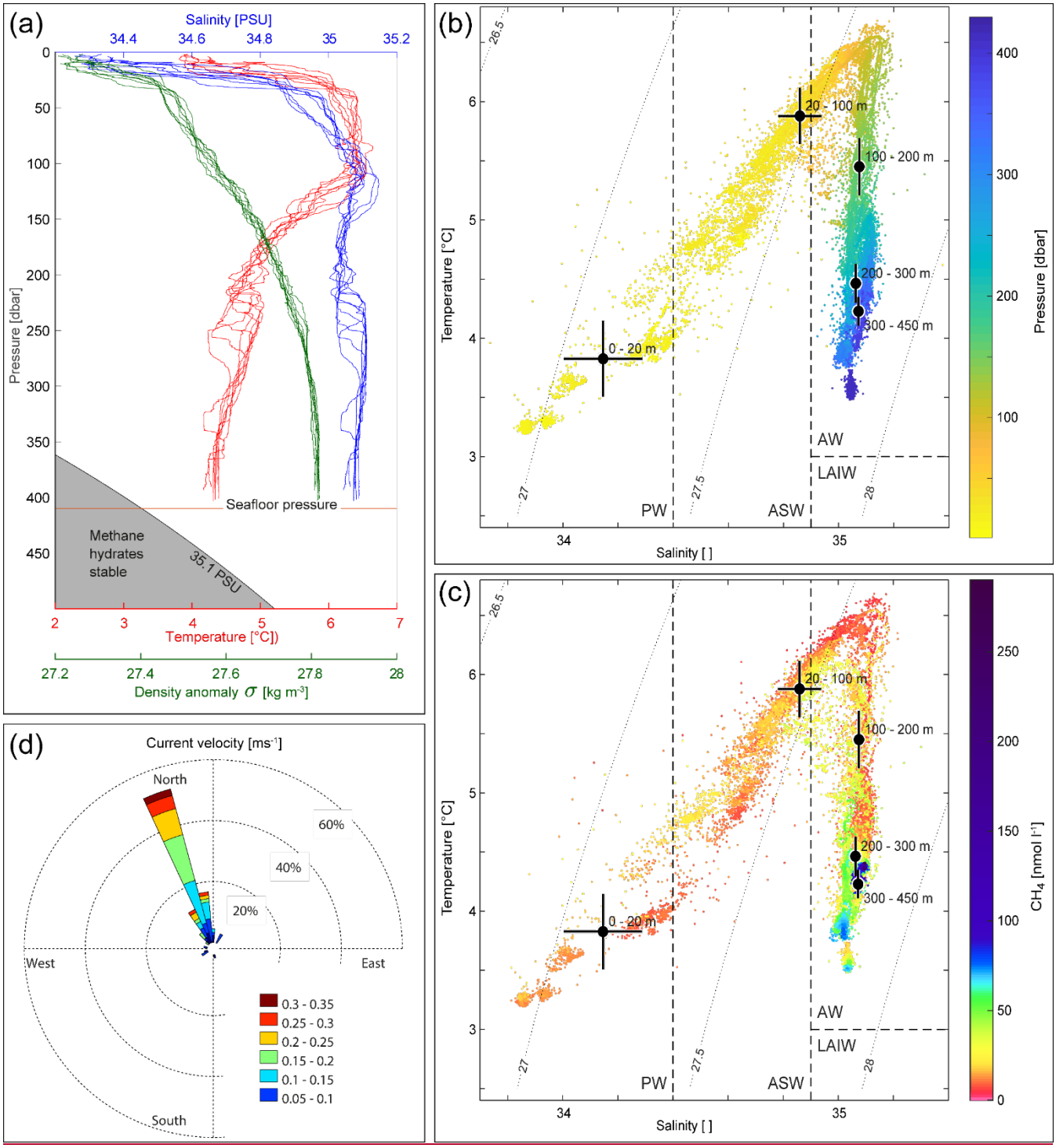

Figure 2. Hydrography during the survey. a) CTD casts 1617- 1626 showing temperature (red), salinity (blue) and density anomaly (green) calculated with Gibbs ~~sweater~~seawater package (McDougall and Barker, 2011). b) Temperature and salinity (TS) diagram coloured by pressure (dbar). Grey curved lines in the background indicate isopycnals (constant density (σ) lines). AW indicates Atlantic Water, PW is polar water, ASW is arctic surface water and LAIW is Lower Arctic Intermediate Water. Water mass definitions are described in the text. Black dots indicate the mean water properties for the different layers and crosses indicate the corresponding standard deviations. c) TS diagram coloured by CH_4 concentrations (nmol l^{-1}) measured with the MILS. Black dots depict average temperature and salinity at water depth intervals, and the error bars indicate the corresponding standard deviations. d) Water currents inferred from inclination of flare spines (Veloso et al., 2015) with a mean bubble rising speed of 23 cm s^{-1}.

3.2 Measured and modelled CH_4 distribution

The high-resolution dissolved CH_4 concentration profiles resulting from towing the MILS along five lines, approximately 15 meters above the seafloor (masf) show high variability (Fig. 3), especially over line 3, which geographically matches the clustering of bubble plumes (Fig. 1a).

On the landward side (lines 1 and 5), the concentration is relatively smooth with an average of ~55 nmol l^{-1}, but along line 5, which is closer to the main seepage area, the concentration is influenced by the nearby seepage, inferred from the concentration peaks reaching up to 105 nmol l^{-1} at 78°33.5' N. On the offshore side, the mean concentrations are 15 and 36 nmol l^{-1} along lines 4 and 2, respectively with elevated CH_4 concentrations of up to ~ 70 nmol l^{-1}, lacking hydroacoustic evidence of CH_4 seep sources. The peak in line 4 may be explained by its proximity to the main bubble seep cluster, but the CH_4 concentrations show more variability along line 2, the offshore-most horizontal trajectory of the survey, which may indicate undetected CH_4 seepage located deeper than 400 mbsl.

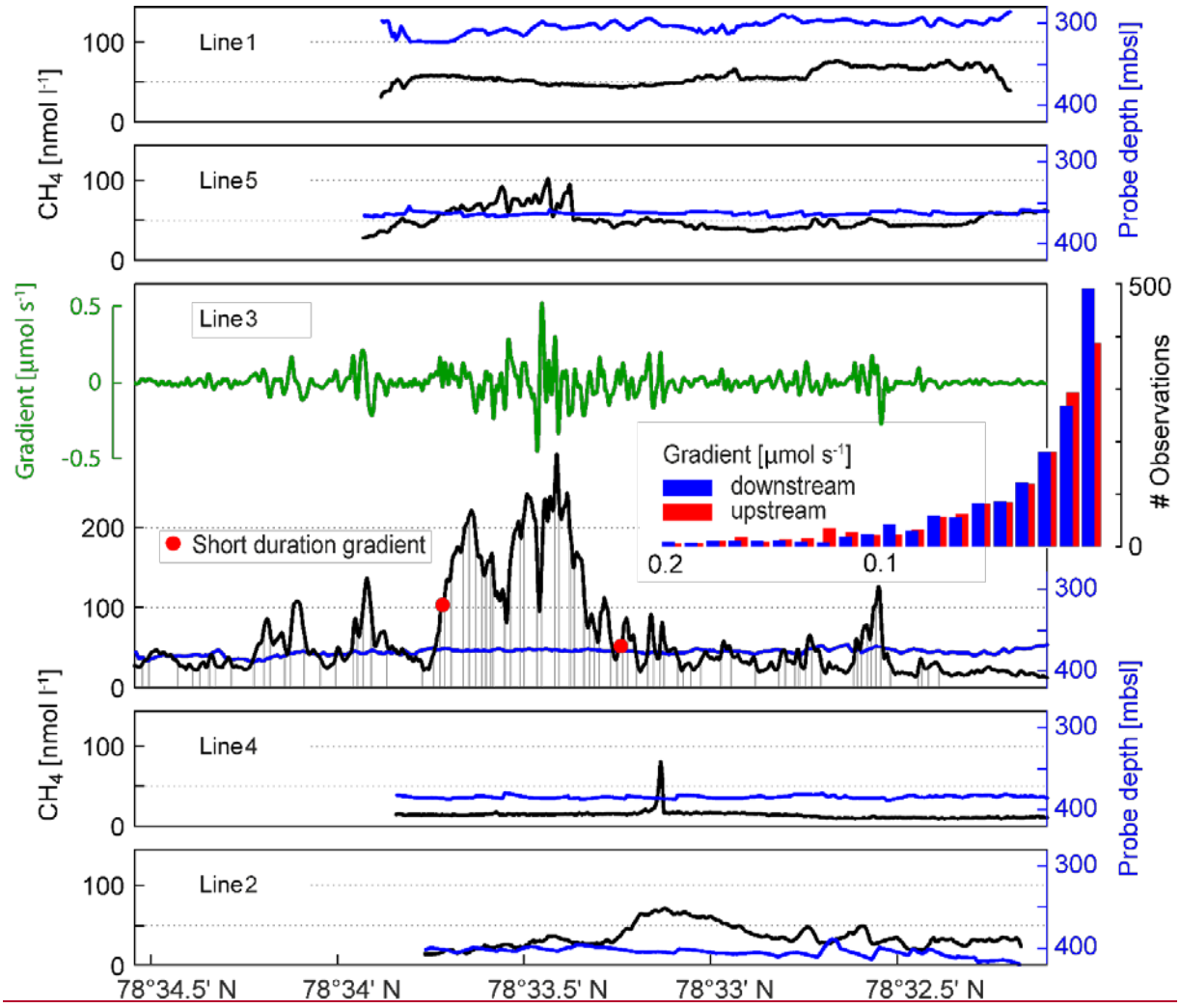

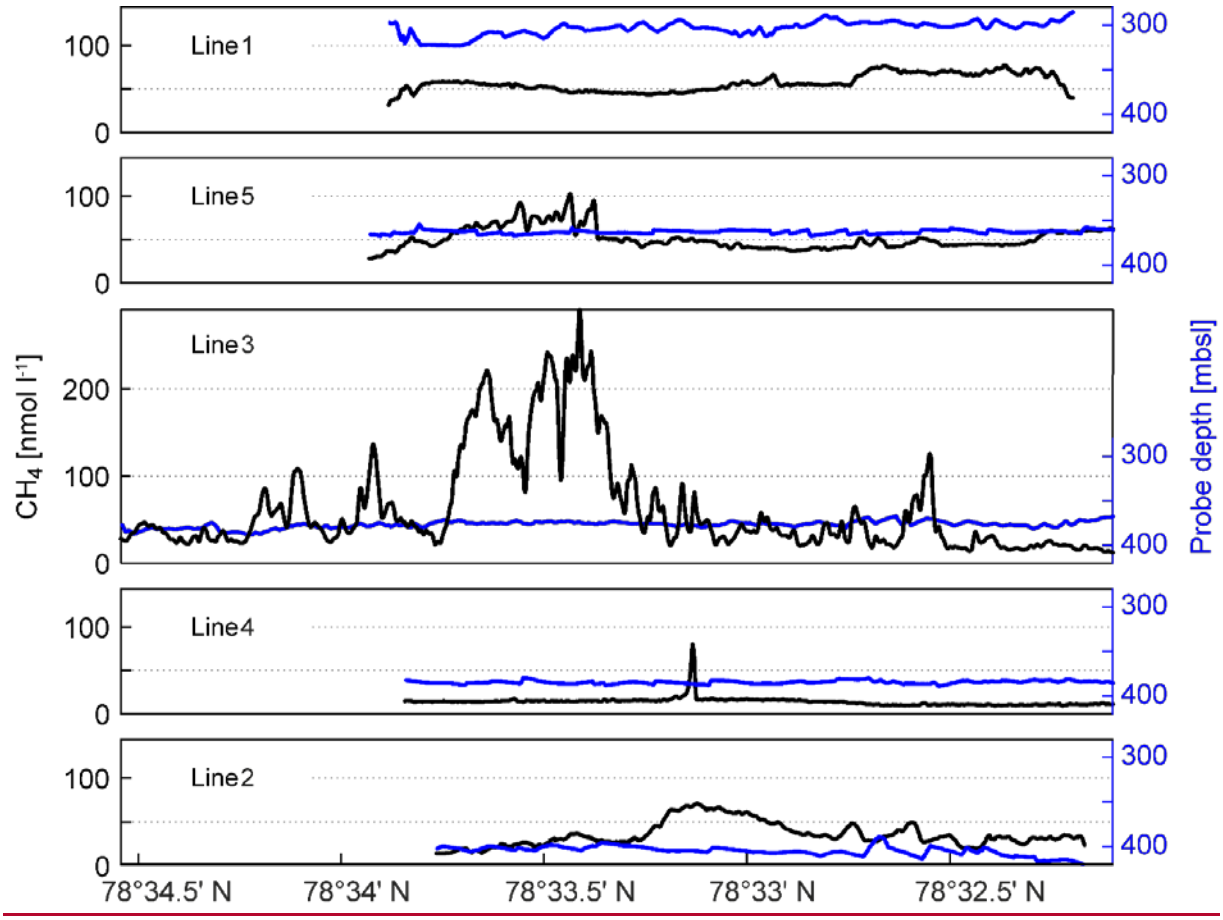

Figure 3. MILS measurements along the five lines ~15 m from the seafloor. Panels show data acquired along lines 1–5, shown in order of proximity to the shore, with line 1 closest to the shore and line 2 furthest offshore. See Fig. 1a for line locations. Black lines show CH_4 concentrations, blue lines show the probe depth. ~~**The concentration gradient along line 3 is shown with a green line and the red- and blue bar chart indicates its probability distribution. Grey vertical lines indicate the slopes chosen for calculation of the mean gradients away from the CH_4 sources. Red dots indicate instances where concentrations changed during periods shorter than the MILS response time and thus, where the concentration gradients are possibly limited by the instrument response time.**~~

A 25-minute down- and upward sequence obtained from the vertical MILS cast at station 1616 (Fig. 4~~),~~) shows excellent repeatability after correcting for ~~an~~the instrument time lag of 15 seconds~~, representing the time required for the gas mixture to reach the measurement cell.~~. The sensor showed no memory effects, i.e. different response ~~time~~times between increased and decreased CH_4 concentrations.

Analysis of discrete samples (DS) from CTD casts 1618 and 1619 and the vertical MILS cast 1616 give further insights to the heterogeneity and temporal variation of the dissolved CH_4 distribution (Fig. 4). Discrete measurements from CTDs 1618 and 1619 reveal a qualitative match with the MILS measured concentrations extracted from line 3 near these stations (red and green symbols in Fig. 4). Discrepancies between the MILS cast 1616 and the DS from CTDs 1618 and 1619 close to the seafloor is likely due to the difference in sampling location, as the MILS vertical cast 1616 was ~150 and ~180 m away from CTDs 1618 and 1619, respectively.

The exponential “dissolution” function, which represents the expected trace of dissolved CH_4 in the water column, resulting from bubble dissolution, was compared to the entire MILS dataset by plotting CH_4 concentrations against height above the seafloor, determined from position corrected pressure and previously acquired multibeam data (Fig. 4).

Elevated CH_4 concentrations at ~160 and ~220 mbsl revealed by the MILS vertical profile 1616 was not identified with DS from the nearby CTD cast 1619, and DS from CTD 1618 reveal only a small fraction of the CH_4 anomaly, because of too sparse sampling (Fig. 4). The MILS data collected 15 masf along line 3 reveals 50 nmol CH_4 l^{-1} while the vertical profile only 30 metres away (MILS-cast 1616), measured ~200 nmol CH_4 l^{-1} (Fig. 4). This emphasizes the strong spatiotemporal variability of the CH_4 distribution in the area.

Despite the high CH_4 variability in the horizontal profiles (Fig. 3), further analysis of the data may be obtained by focusing on line 3, towed in north-south direction at ~0.8 m s^{-1} directly over the bubble streams. Based on a mean depth of 390 m and the depth of the towed CTD, the height above the seafloor of the towed probe along line 3, was 13.4 ± 3.8 m. The fast response time of the MILS sensor (T_{90} = 15 s) revealed decametre-scale variations of the dissolved CH_4 concentrations with high values well correlated with the echosounder signal, after correcting for the towed instrument position (Fig. 5).

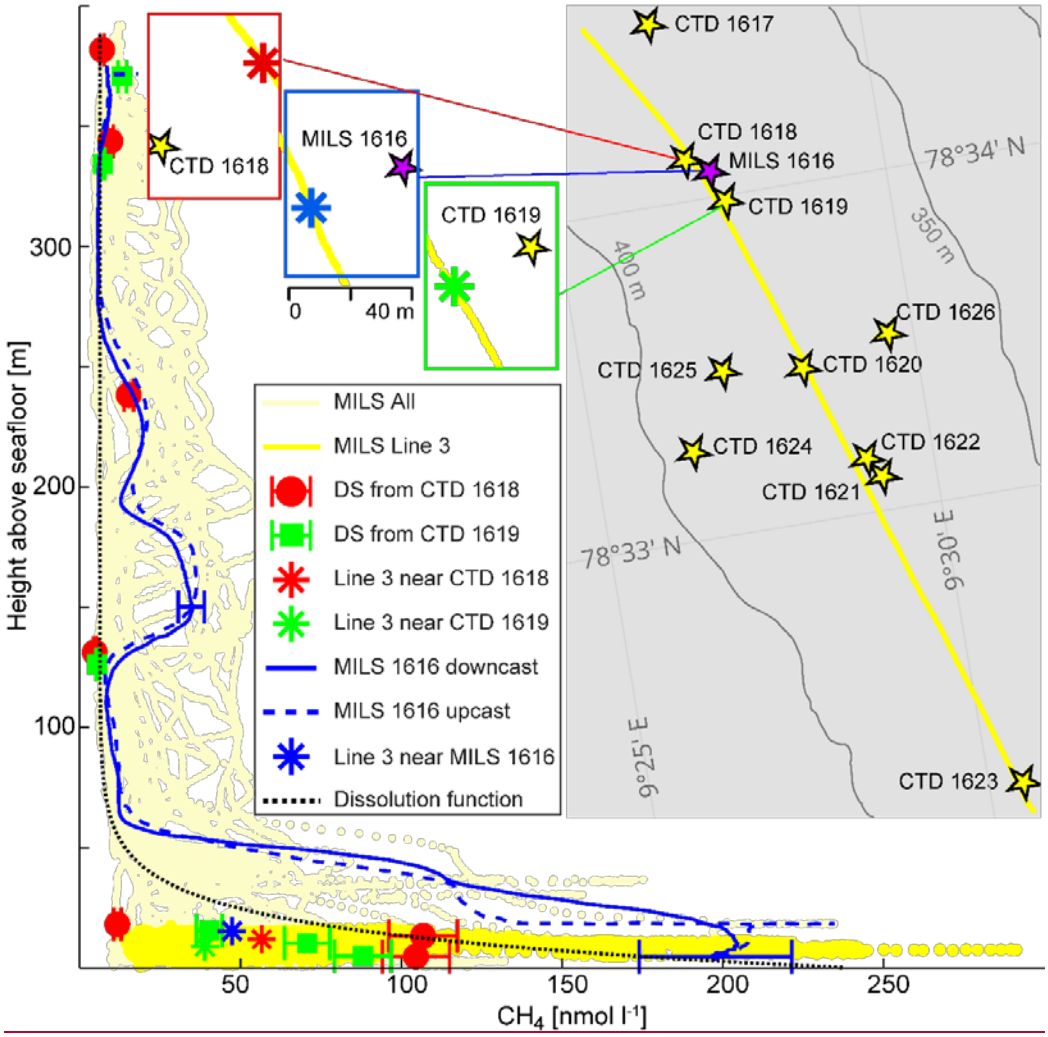

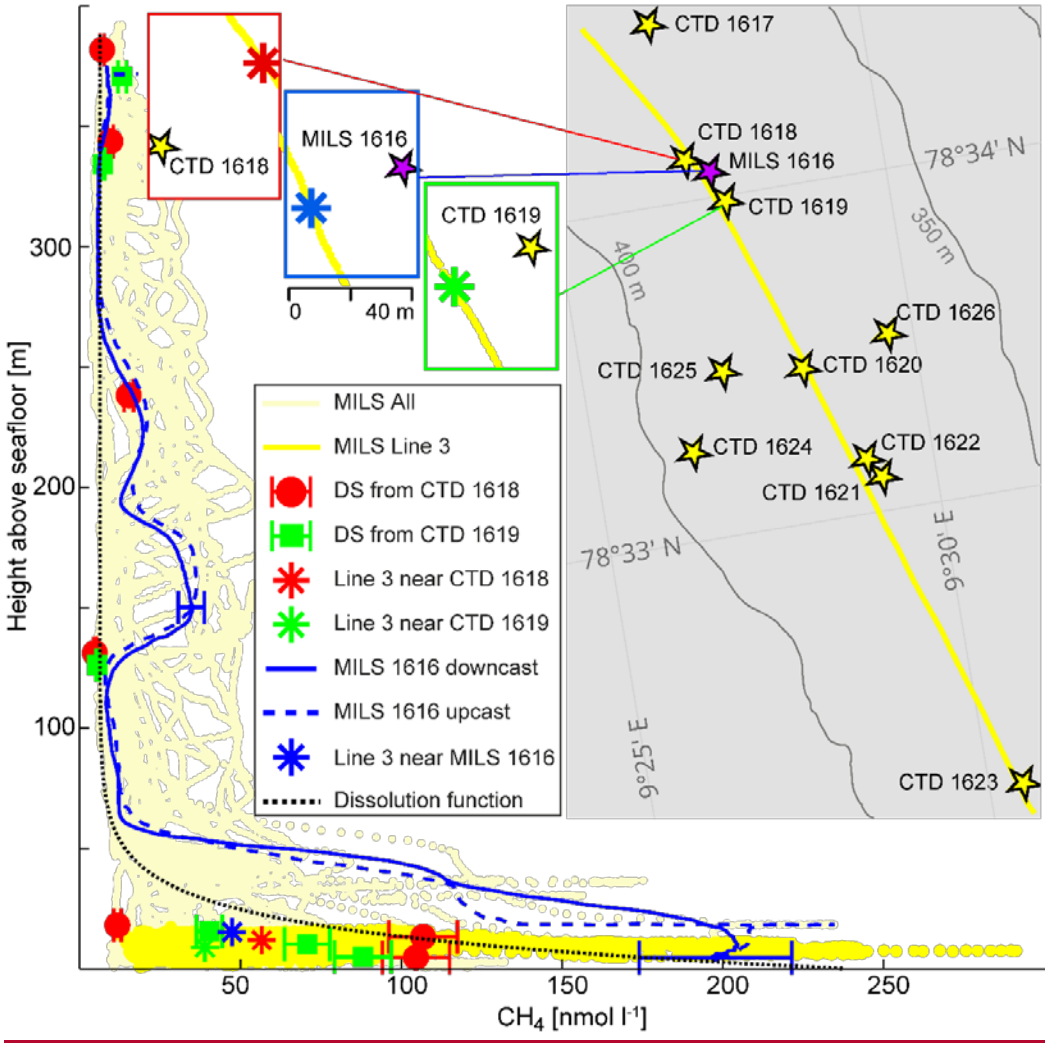

Figure 4. High-resolution CH_4 concentrations and discrete samples. Light yellow lines show CH_4 concentrations acquired with the MILS during the entire survey and the bright yellow derives from line 3 at ~15 masf only. Solid and dashed blue lines represent continuous down- and upward profiles acquired at station 1616 after correction for instrument response time. The blue error bars indicate the instrument uncertainty of 12%. Discrete sample data is shown as red dots (CTD 1618) and green squares (CTD 1619) with error bars that indicate the discrete sampling/ headspace GC method uncertainty of 4%. The asterisks indicate MILS data points from the towing along line 3, closest to the vertical cast 1616 (blue), to CTD 1618 (red) and CTD 1619 (green). The black dotted line indicates the exponential dissolution function described in the text. The inset map shows the locations of the CTDs with discrete sampling (stnr1617–1623) (yellow stars) as well as line 3, which is indicated with a yellow line. The blue rectangle shows the location of the vertical MILS profile from ~~stnr1616~~station 1616 (purple star) and the data point from line 3, which is closest to the deepest location of the vertical cast (blue asterisk). The green rectangle shows the location of CTD 1619 and the closest point on line 3 (green asterisk), while the red rectangle shows the location of CTD 1618 and the corresponding point on line 3 (red asterisk).

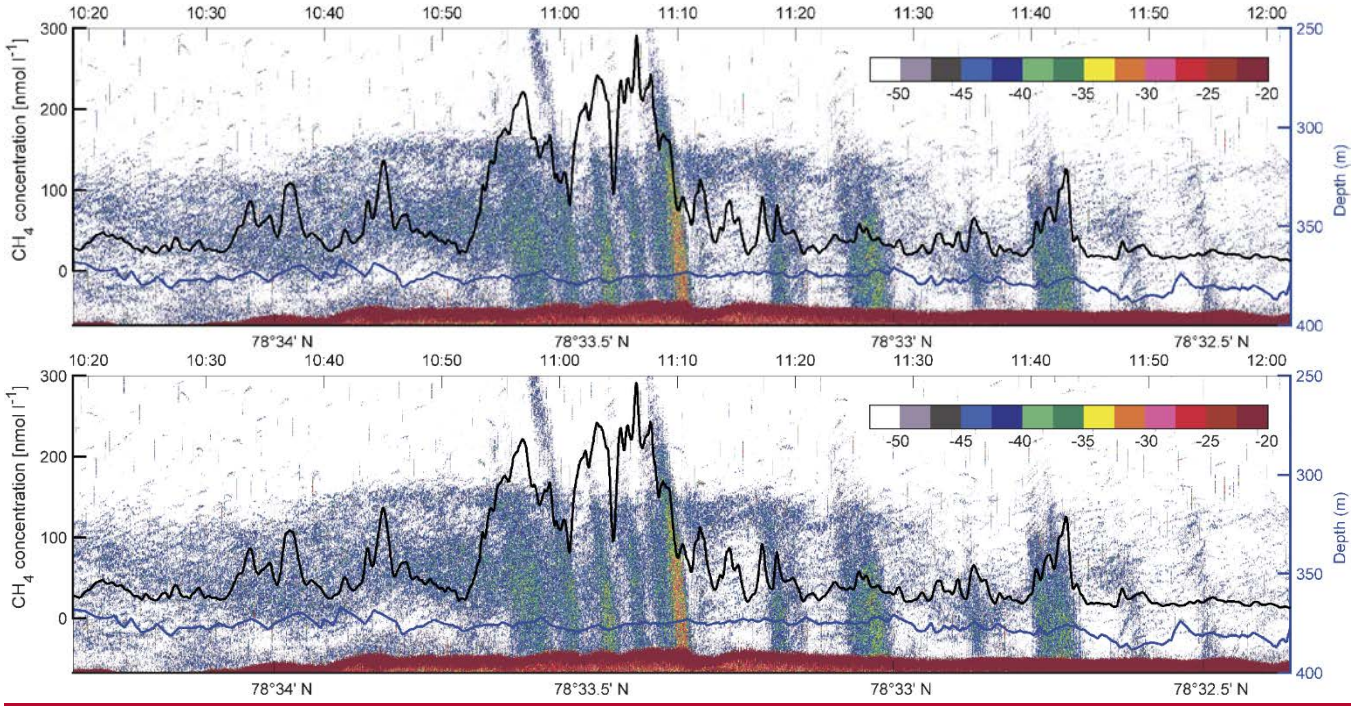

Figure 5. Towed MILS data overlying echo-sounder data. The black line shows the CH_4 concentration along line 3 (see Fig. 1 for location) at ~15 m from the seafloor. The blue line indicates the depth of the probe. The echogram, displaying TS values (colour bar shows intensity (-dB)) from the 38 kHz-channel of the EK60, is shown in the background.

A close analysis of the measured concentration reveals that the up- and down- stream gradients are equally distributed (bar chart in Fig. ~~3~~SI 2c). This symmetry suggests that CH_4 disperses fast and equally in all horizontal directions around the bubble plumes while being advected away from the source.

The measured CH_4 concentrations along line 3 changed significantly (5% or more) on sub-response times (<15 s) in only two instances and over a total time of 26 s, out of 1h 42 min, as indicated with red dots in Fig. ~~3~~SI 2a. This suggests that the MILS resolved 99.6% of the gradients and that the response time of the MILS did not limit the resolution of the CH_4 distribution. The mean absolute gradient, assessed from steadily increasing or decreasing concentrations (grey vertical lines in Fig. ~~3~~SI 2a show the position of the selected slopes), was 1.5 nmol l^{-1} m^{-1}, corresponding to 1.2 nmol l^{-1} s^{-1}. The minimum and maximum lateral gradients were -5.0, and 4.8 nmol l^{-1} m^{-1}, which corresponds to -4.1 and 4.6 nmol l^{-1} s^{-1}. Correlations of CH_4 concentrations versus depth and speed changes were low (R= 0.0133, -0.0001, -0.0094, 0.0028 for ship speed, ship acceleration, vertical instrument speed and instrument acceleration, respectively), showing the stability of the instrument during rapid movements and disproving artefacts due to water flow fluctuations at the membrane.

Sources of CH_4 constraining the control volume and 2D model were obtained from the acoustic mapping and quantification described in section 2.4. During the entire survey, we identified 68 unique groups of bubble plumes, with an average flow rate of 48 (SD = 50) ml min^{-1}. Within 50 metres of line 3, we acoustically identified 31 flares with an average flow rate of 60 -(SD = 65) ml min^{-1} amounting to a total flow rate of 1.87 l min^{-1}. These flow rates were taken as sources in the control volume and 2D model. ~~Flarehunter~~FlareHunter calculates the flow rates in a layer 5–10 m above the seafloor. In order to calculate flow rates from the seafloor, we upscaled the ~~Flarehunter~~FlareHunter flow rates by 40% to compensate for bubble dissolution near the seafloor, in accordance with the dissolution profile.

The 2D model was run to steady state with different diffusion coefficients, $k \in [0.3 - 4.9\ m^2\ s^{-1}]$, adopted from dye-experiments offshore Rhode Island (Sundermeyer and Ledwell, 2001). These coefficients are in agreement with the ones obtained from the Celtic Sea ($k \in [0.8 - 4.4\ m^2\ s^{-1}]$) (Stashchuk et al., 2014), but much higher than the coefficient applied by Graves et al. (2015) ($k = 0.07\ m^2\ s^{-1}$). The best fit between the 2D model and the MILS data (R = 0.68) was achieved during a simulation with k = 1.5 $m^2\ s^{-1}$. Because the high-end coefficients of Sundermeyer and Ledwell (2001) and Stashchuk et al. (2014) were derived during wavy conditions, and because our model mainly resolves the near-bottom region, away from wave action, we interpret that our best-fit diffusion coefficient is relatively high. The resulting range of model outputs and the best fit-model simulation are visualized and compared with high-resolution measurements in Fig. 6. Despite applying a high diffusion coefficient, the 2D model shows a residual downstream tailing, which is not seen in the MILS data. We attribute this to the fact that the model does not resolve small scale eddies, but only diffusion across the domain and diffusion/ advection along the domain.

The salinity and temperature profiles of the towed CTD indicate well-mixed water, particularly over the most prominent gas flares. Here, the relative standard deviation of the salinity and temperature ~~and salinity~~ drops by ~~a factor of four~~factors of 10, and 58 respectively, as highlighted by the dashed-line box in Fig. ~~6~~6. The depth stability of the probe is also better in the area. Its relative standard deviation dropped by a factor of 3, which is not enough to justify the larger factors observed for the temperature and salinity. We interpret that this is caused by turbulent mixing enhanced by the bubble streams.

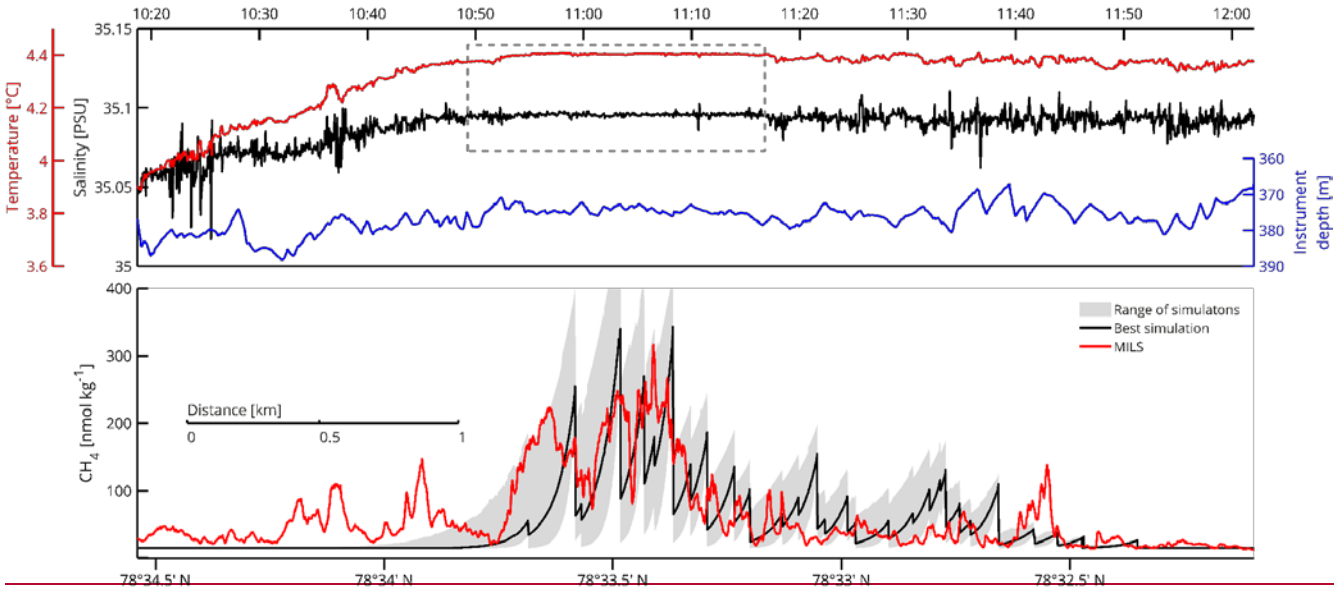

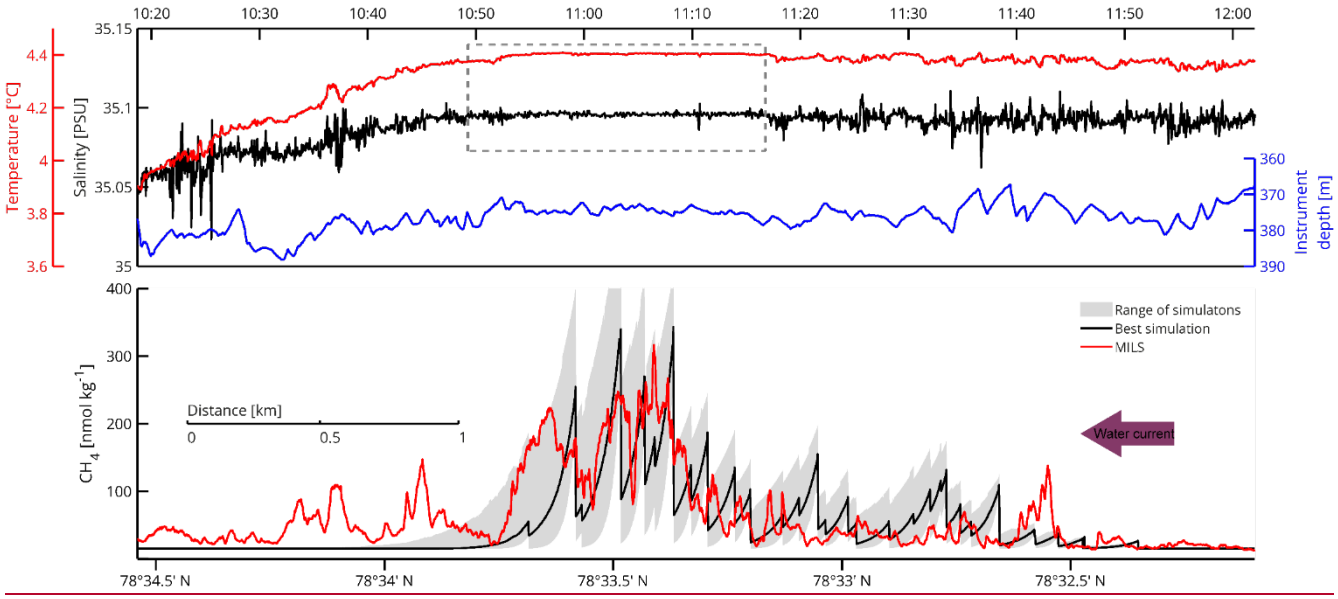

Figure 6. Water properties and comparison between modelled and measured dissolved CH_4 concentrations along line 3. Top panel shows temperature and salinity data together with the depth of the towed instruments. The dashed-line box highlights the area of intense mixing. In the lower panel, the red line shows the dissolved CH_4 measured by the MILS. The grey area indicates the range of CH_4 concentrations from the 2D model simulations. The black line depicts output of the model simulation with the best match with the measured concentrations.

3.3 Methane inventory

The method, dimensions, and resolution chosen for calculating CH_4 inventories may strongly influence the resulting content and average concentrations. This may have serious implications when the results are used for upscaling. To highlight this, we applied different inventory calculation methods on the same water volume.

Averages along line 3 were calculated from: a) Concentrations from discrete sampling, based on different sampling depths. b) Discrete data from different depths, linearly interpolated along the line. c) High-resolution data obtained from the MILS data ~15 masf. d) Concentrations extracted from the 2D model output at steady state at 15 masf.

Average concentrations were calculated in a "box" volume equivalent to MILS line 3 (4.5 km long (x-direction), 50 m wide (y-direction), equivalent to the echosounder beam width, 75 m high (z-direction) corresponding to the most dynamic and CH_4 enriched zone (e.g. McGinnis et al., 2006; ~~Graves et al., 2015;~~ Jansson et al., 2019;Graves et al., 2015). Box averages were derived as follows: The volume was divided into 1 m cubic cells. Cells located in the y-centre and in z-positions vertically matching the underlying data (DS or MILS) were populated with the MILS, or interpolated DS profiles. The remaining cells were populated by perpendicular and vertical extrapolation following the typical horizontal gradient of 1.5 nmol l^{-1} m^{-1}, and vertical dissolution profiles scaled by the measured or interpolated concentrations. The mean concentrations from the 2D model was delimited by the height of the box. The control volume model provided only one value for the entire box.

The underlying data and its interpolation is seen in Fig. 7 and the resulting averages are reported in Table 1.

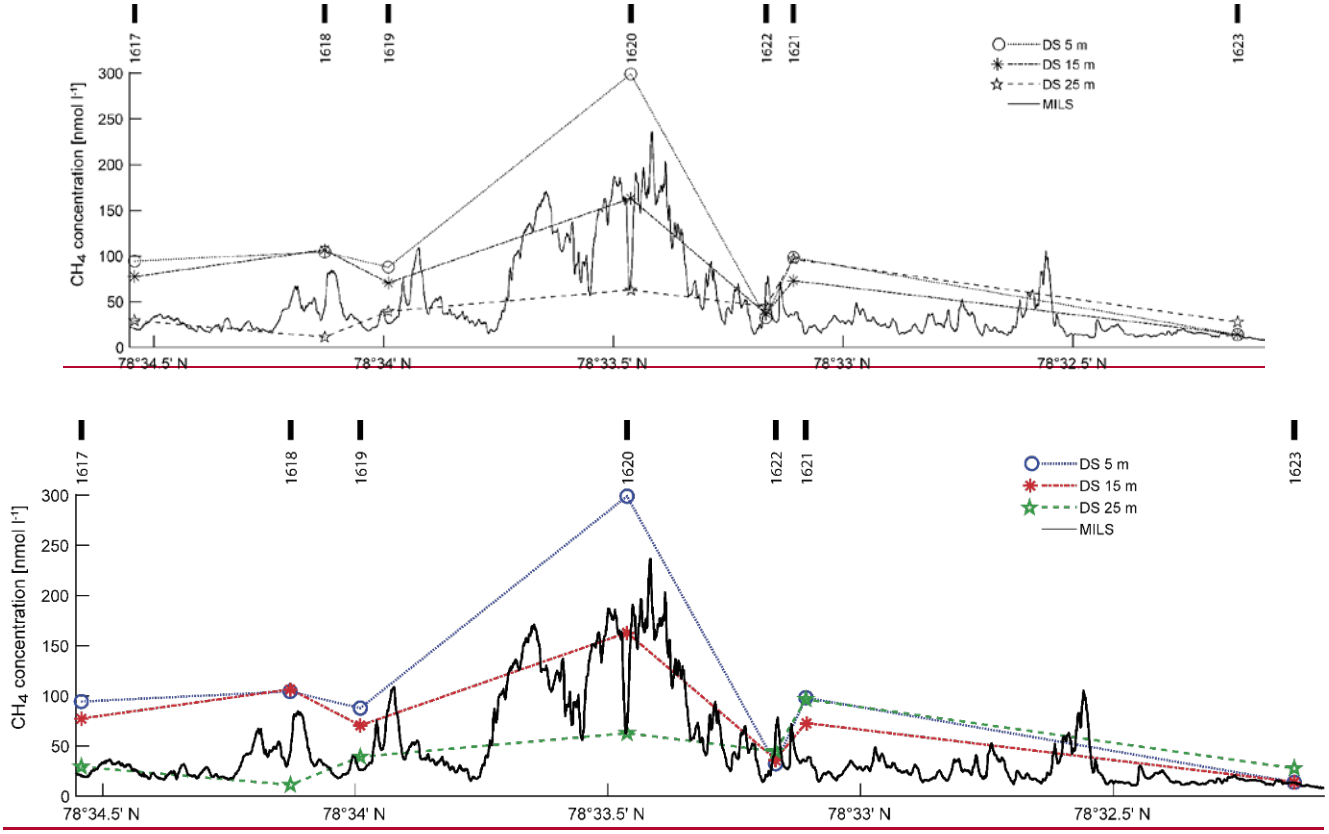

Figure 7: Underlying CH_4 concentration data for inventory calculations. Solid black line shows the continuous MILS profile ~15 masf along line 3. DS concentrations at various depths are shown as blue circles, red asterisks and green stars for 5, 15 and 25 masf respectively, and blue dotted, ~~dashed, and~~red dash-dotted, and green dashed lines represent the corresponding linear horizontal interpolations. CTD cast numbers are marked with thick black lines at the top of the graph.

The average CH_4 concentration in the box volume based on continuous data is similar to the average obtained from discrete data at 15 m above the seafloor. We obtained 47 vs 77 nmol l^{-1} for the high-resolution line and the interpolated DS, while the box averages for the high-resolution and interpolated DS were 22 vs 29 nmol l^{-1}. The 2D model yielded a line average of 60 nmol l^{-1}, while it was 22 nmol l^{-1} for the box. The control volume model predicted a steady state concentration of 23 nmol l^{-1} when the diffusion coefficient of 1.5 m^2 s^{-1}, inferred from the 2D model was applied.

4 Discussion

During our survey, the mean flow rate at the seafloor per flare within 50 m of line 3, was 84 (SD = 91.6) ml min^{-1}, (min = 15.8, max= 355.6 ml min^{-1}). This is comparable with the flow rate per flare of 125 ml min^{-1}, estimated by Sahling et al. (2014) who assumed that an acoustic flare consists of 6 bubble streams, each with a flow rate of 20.9 ml min^{-1}. The authors found 452 flares in the area, for which they assumed similar flow rates, and thereby calculated a total flow in the area of ~57 l min^{-1}. Our study encompasses a smaller area, where we only detected 68 flares (31 flares within 50 m of line 3) and the total flow rate from these 68 flares was 4.56 l min^{-1}. ~~This total flow translates to 65.7 t CH_4 y^{-1} assuming constant ebullition, which may be compared to CH_4 seepage of ~150 t CH_4 y^{-1} estimated for a larger area by Veloso et al. (2019)~~This total flow translates to 65.7 t CH_4 y^{-1} assuming constant ebullition. Considering the sparse beam coverage and relatively small area, this may be compared to CH_4 seepage of ~550 t CH_4 y^{-1} estimated for a larger area, covered by 9 surveys (Veloso et al., 2019b), and ~400 t CH_4 y^{-1}

(Sahling et al., 2014), in a study area covering ours, but also extending northwards, where additional gas venting occurs. A comparison of studies from the same area, using different methods, shows a large range of yearly CH_4 emissions to the water column. Flow rates of CH_4 per ~~metre of~~distance along the continental shelf from previous studies given by the authors (900 kg m^{-1} y^{-1} (Westbrook et al., 2009); 141 kg m^{-1} y^{-1} (Reagan et al., 2011); 13.8 (6.9–20.6) t m^{-1} y^{-1} (Marín-Moreno et al., 2013); 2400 (400–4500) mol m^{-1} y^{-1} (Sahling et al., 2014); 748 (561–935) t m^{-1} y^{-1} (Berndt et al., 2014)) yield emissions of 4050, 635, 992, 173 and 54000 t CH_4 y^{-1} over the 4500 m section of the continental shelf which corresponds to our line 3.

The MILS data collected 15 masf along line 3 did not reveal the high concentrations (~200 nmol l^{-1}) measured during the vertical cast only 30 m away, emphasizing the heterogeneous CH_4 distribution, and highlighting the need for high-resolution sensing, rather than sparse discrete sampling.

The fast response of the MILS helped revealing decametre scale variability of dissolved CH_4, and we conclude that uncertainties introduced by MILS response time were negligible in this survey. The observed symmetry of CH_4 gradients suggests fast dispersion in all horizontal directions while enriched water is advected away from the sources.

Because the instrument assembly lacked an inertia measurement unit, the stability during towing is unknown, but we did not observe any effect on the measurements from wobble and/ or rotation.

Gentz et al. (2014) and Myhre et al. (2016) suggested that a pronounced pycnocline is a prerequisite to limit the vertical transport of dissolved CH_4 towards the surface. One should note that this hypothesis was based on discrete sample data, rather than high-resolution data. We observed high CH_4 concentrations up to 75–100 masf, which is in agreement with bubble models (e.g. McGinnis et al., 2006; Jansson et al., 2019), highlighting that bubbles of observed sizes (~3 mm average equivalent radius) are fully dissolved within this range. Density stratification plays an important role in the vertical distribution of dissolved CH_4 because turbulent energy is required to mix solvents across isopycnals. Vertical mixing is therefore inhibited even without the presence of a strong pycnocline. We suggest that the observed height limit is a result of rapid bubble dissolution and inefficient vertical mixing, regardless of the existence of a pronounced pycnocline.

We observed CH_4 concentrations of up to 100 nmol l^{-1} without the acoustic signature of flares north of the active flare zone (Fig. 5). Echograms from the CAGE 15-6 survey (this work) and previous surveys conducted in 2010 (AOEM 2010 cruise, University of Tromsø, with ~~R/V~~RV Jan Mayen) and 2013 (CAGE 13-7 cruise, with RV Helmer Hanssen ~~(e.g. Portnov et al., 2016)~~(e.g. Portnov et al., 2016)) reveal that the nearest bubble stream is located ~300 m northeast of this CH_4 anomaly. Several hypotheses may explain this CH_4 enrichment: a) nearby presence of CH_4 enriched water seepage (hypothetically from dissociating hydrates) from the seafloor; b) presence of bubble streams with bubbles too small to be detected by the echosounder (the detection limit (TS<-60 dB) of a single bubble was 0.42 mm for this survey~~;~~); c) advection of CH_4-enriched water from an upstream bubble plume source, not detected by the echosounder. In our case, the temperature- and salinity anomaly, which coincides with the increased CH_4, reveals mixing of AW with colder and fresher water (Fig. 6). Because mixing lines drawn in the TS diagrams (Fig. 2b and 2c) point towards PW rather than a pure fresh water source, our data

supports hypothesis c, namely that AW mixed with PW was transported ~~downslope and downstream with the WSC, and was,~~ and enriched in CH_4 while passing over a bubble plume before reaching the location of the measurement. Lateral eddies or bottom Ekman transport may have been responsible for the intrusion of fresh, cold, CH_4 enriched water.

The 2D model relies on ~~known~~acoustically detected bubble plume locations, and the difference between measured and modelled CH_4 is obvious along line 3 from 10:30 to 10:50 as seen in Fig. 6. The CH_4 signal from high-resolution data, not thoroughly resolved by the model, underscores that mapping and modelling based on echosounder data are not enough for a correct quantitative estimate of the CH_4 inventory. The 2D model required a high diffusion coefficient in order to reproduce the variability of measurements, which is supported by high turbulence in the area, caused by the strong currents. Downstream tailing of CH_4 concentrations seen in the 2D model was not observed with the MILS. In fact, MILS data reveal equal distribution of down-and upstream concentration gradients. We explain the discrepancy by the fact that the 2D model does not resolve eddies and the CH_4 source is placed in discrete cells, following a theoretical straight bubble line, and not accounting for diffusion along the bubble paths.

The relatively high midwater (120–260 mbsl) CH_4 concentrations revealed by the vertical MILS cast 1616 was only partly observed in the discrete sampling and was not inferred from echosounding. We suggest that this discrepancy is attributed to seepages at the corresponding depth interval, not previously mapped. The closest known seepages are a few km away from the location, at the shallow shelf (50–150 mbsl) and at the shelf-break (~250 mbsl) (Veloso et al., 2015), but it is doubtful that water masses from these locations can reach the surveyed area, as the WSC is persistently northbound. Unless horizontal eddies transport CH_4 from the shelf-break to this area, this result indicates the existence of undiscovered CH_4 bubble plumes further south, at the depth of the observed anomaly.

The high-resolution data from the MILS results in a significantly lower CH_4 inventory than the one obtained from discrete sampling (47 vs 77 nmol l^{-1}) due to the heterogeneous distribution of dissolved CH_4. The choice of discrete sample locations can significantly affect the resulting average concentration. The average CH_4 concentration (93 nmol l^{-1}) estimated by Graves et al. (2015) from a box with dimensions Δx = 1m, Δy = 50 m, Δz = 75 m, obtained from a DS transect across the slope, was substantially higher than our box estimates of 20–39 nmol l^{-1}. These two results highlight the need for high-resolution sensing when estimating CH_4 inventories and average CH_4 concentrations.

The optical spectrometer of the MILS can be tuned or replaced to improve its sensitivity or to sample more CH_4 enriched waters. We believe the MILS would be an excellent tool for evaluating CH4 related water column processes. Grilli et al. (2018) reported a sensitivity of ±25 ppbv in air, which translates to ±0.03 nmol l^{-1} at 20 °C and a salinity of 38, which is low enough for investigations of atmospheric exchange and CH4 production/ consumption rates.

5 Conclusion

We have presented new methods for understanding the dynamics of CH_4 after its release from the seafloor, coupling for the first time continuous high-resolution measurements from a reliable and fast CH_4 sensor (MILS) with dedicated models. The

MILS sensor was successfully deployed as a towed body from a research vessel and provided high-resolution, real-time data of both vertical and horizontal dissolved CH_4 distribution in an area of intense seepage west of Svalbard. For the first time, we observed a more heterogeneous CH_4 distribution than has been previously presumed.

We employed an inverse acoustic model for CH_4 seepage mapping and quantification, which provided the basis for a new 2D model and a new control volume model, which both agreed relatively well with observations. The 2D model did not reproduce the symmetric gradients observed with the MILS, which suggests a need to improve the model by including turbulent mixing enhanced by the bubbles streams.

Despite the large spatial and temporal variability of the CH_4 concentrations, a comparison between high-resolution (MILS) and DS data showed good general agreement between the two methods.

Heterogeneous CH_4 distribution measured by MILS matched acoustic backscatter, except for an area with high CH_4 concentrations without acoustic evidence of CH_4 source. Similarly, high midwater CH_4 concentration was observed by the MILS vertical casts with little evidence of a nearby CH_4 source, further supporting that high-resolution sensing is an essential tool for accurate CH_4 inventory assessment and that high-resolution sensing can give clues to undetected sources.

CH_4 inventories, given by discrete sampling agreed with those from high-resolution measurements, but sparse sampling may over- or underestimate inventories, which may have repercussions if the acquired data is used for predicting degassing of CH_4 to the atmosphere in climate models. The added detail of the fine structure allows for better inventories, elucidates the heterogeneity of the dissolved gas, and provides a better insight to the physical processes that influence the CH_4 distribution.

The methods for understanding CH_4 seepage presented here shows potential for improved detection and quantification of dissolved gas in oceans and lakes. Applications for high-resolution CH_4 sensing with the MILS include environmental and climate studies as well as gas leakage detection desired by fossil fuel industry.

6 Data availability

A dataset comprising the MILS sensor data and echosounder files is available from the UiT Open Research Data repository https://doi.org/10.18710/UWP6LL.

7 Author contribution

PJ and JT contributed equally to the work leading to this manuscript, and are listed alphabetically. JM and JC initiated the collaboration and designed the study. JT, RG, PJ, and JM planned and participated in the field campaign. JT and RG systematized and synchronized the high-resolution MILS data. PJ mapped and quantified gas seepage and water currents by collecting and analysing echosounder data. PJ collected and analysed the CTD data and water samples~~.~~, and organized the data repository. RG converted mixing ratios to aqueous concentrations. PJ developed the numerical models. AS analysed the water mass properties. JT and PJ calculated CH_4 inventories. All authors contributed to the manuscript.

8 Acknowledgements

The research leading to these results has received funding from the European Community's Seventh Framework Programs ERC-2011-AdG under grant agreement n° 291062 (ERC ICE&LASERS), as well as ERC-2015-PoC under grant agreement n° 713619 (ERC OCEAN-IDs). Additional funding support was provided by SATT Linksium of Grenoble, France (maturation project SubOcean CM2015/07/18). The collaboration between CAGE and IGE was initiated thanks to the European COST Action ES902 PERGAMON. The research is part of the Centre for Arctic Gas Hydrate, Environment and Climate (CAGE) and is supported by the Research Council of Norway through its Centers of Excellence funding scheme grant No. 223259. We thank the crew on board RV Helmer Hanssen for the assistance during the cruise, and the University of Svalbard for the logistics support. We also thank three anonymous referees for their suggestions to improve this manuscript.

References

Andreassen, K., Hubbard, A., Winsborrow, M., Patton, H., Vadakkepuliyambatta, S., Plaza-Faverola, A., Gudlaugsson, E., Serov, P., Deryabin, A., Mattingsdal, R., Mienert, J., and Bünz, S.: Massive blow-out craters formed by hydrate-controlled methane expulsion from the Arctic seafloor, Science, 356, 948, doi:10.1126/science.aal4500, 2017.

Berndt, C., Feseker, T., Treude, T., Krastel, S., Liebetrau, V., Niemann, H., Bertics, V. J., Dumke, I., Dünnbier, K., Ferré, B., Graves, C., Gross, F., Hissmann, K., Hühnerbach, V., Krause, S., Lieser, K., Schauer, J., and Steinle, L.: Temporal Constraints on Hydrate-Controlled Methane Seepage off Svalbard, Science, 343, 284, doi:10.1126/science.1246298, 2014.

Biastoch, A., Treude, T., Rüpke, L. H., Riebesell, U., Roth, C., Burwicz, E. B., Park, W., Latif, M., Böning, C. W., and Madec, G.: Rising Arctic Ocean temperatures cause gas hydrate destabilization and ocean acidification, Geophysical Research Letters, 38, doi:10.1029/2011GL047222, 2011.

Boetius, A., and Wenzhöfer, F.: Seafloor oxygen consumption fuelled by methane from cold seeps, Nature Geoscience, 6, 725-734, doi:10.1038/ngeo1926, 2013.

Boulart, C., Prien, R., Chavagnac, V., and Dutasta, J.-P.: Sensing Dissolved Methane in Aquatic Environments: An Experiment in the Central Baltic Sea Using Surface Plasmon Resonance, Environmental Science & Technology, 47, 8582-8590, doi:10.1021/es4011916, 2013.

Boulart, C., Briais, A., Chavagnac, V., Révillon, S., Ceuleneer, G., Donval, J.-P., Guyader, V., Barrere, F., Ferreira, N., Hanan, B., Hémond, C., Macleod, S., Maia, M., Maillard, A., Merkuryev, S., Park, S.-H., Ruellan, E., Schohn, A., Watson, S., and Yang, Y.-S.: Contrasted hydrothermal activity along the South-East Indian Ridge (130°E–140°E): From crustal to ultramafic circulation, Geochemistry, Geophysics, Geosystems, 18, 2446-2458, 10.1002/2016GC006683, 2017.

Damm, E., Mackensen, A., Budéus, G., Faber, E., and Hanfland, C.: Pathways of methane in seawater: Plume spreading in an Arctic shelf environment (SW-Spitsbergen), Continental Shelf Research, 25, 1453-1472, doi:10.1016/j.csr.2005.03.003, 2005.

Dewey, R. K.: Mooring Design & Dynamics—a Matlab® package for designing and analyzing oceanographic moorings, Marine Models, 1, 103-157, doi:10.1016/S1369-9350(00)00002-X, 1999.

Egbert, G. D., and Erofeeva, S. Y.: Efficient Inverse Modeling of Barotropic Ocean Tides, Journal of Atmospheric and Oceanic Technology, 19, 183-204, doi:10.1175/1520-0426(2002)019<0183:EIMOBO>2.0.CO;2, 2002.

Ferré, B., Mienert, J., and Feseker, T.: Ocean temperature variability for the past 60 years on the Norwegian-Svalbard margin influences gas hydrate stability on human time scales, Journal of Geophysical Research: Oceans (1978–2012), 117, doi:10.1029/2012JC008300, 2012.

Gentz, T., Damm, E., Schneider von Deimling, J., Mau, S., McGinnis, D. F., and Schlüter, M.: A water column study of methane around gas flares located at the West Spitsbergen continental margin, Continental Shelf Research, 72, 107-118, doi:10.1016/j.csr.2013.07.013, 2014.

Graves, C. A., Steinle, L., Rehder, G., Niemann, H., Connelly, D. P., Lowry, D., Fisher, R. E., Stott, A. W., Sahling, H., and James, R. H.: Fluxes and fate of dissolved methane released at the seafloor at the landward limit of the gas hydrate stability zone offshore western Svalbard, Journal of Geophysical Research: Oceans, 120, 6185-6201, doi:10.1002/2015JC011084, 2015.

Greinert, J., Artemov, Y., Egorov, V., De Batist, M., and McGinnis, D.: 1300-m-high rising bubbles from mud volcanoes at 2080m in the Black Sea: Hydroacoustic characteristics and temporal variability, Earth and Planetary Science Letters, 244, 1-15, doi:10.1016/j.epsl.2006.02.011, 2006.

Grilli, R., Triest, J., Chappellaz, J., Calzas, M., Desbois, T., Jansson, P., Guillerm, C., Ferré, B., Lechevallier, L., Ledoux, V., and Romanini, D.: Sub-Ocean: Subsea Dissolved Methane Measurements Using an Embedded Laser Spectrometer Technology, Environmental Science & Technology, 52, 10543-10551, doi:10.1021/acs.est.7b06171, 2018.

Hong, W. L., Torres, M. E., Portnov, A., Waage, M., Haley, B., and Lepland, A.: Variations in Gas and Water Pulses at an Arctic Seep: Fluid Sources and Methane Transport, Geophysical Research Letters, 45, 4153-4162, doi:10.1029/2018GL077309, 2018.

Jansson, P., Ferré, B., Silyakova, A., Dølven, K. O., and Omstedt, A.: A new numerical model for understanding free and dissolved gas progression toward the atmosphere in aquatic methane seepage systems, Limnology and Oceanography: Methods, 0, doi:doi:10.1002/lom3.10307, 2019.

Judd, A., and Hovland, M.: Seabed fluid flow: the impact on geology, biology and the marine environment, Cambridge University Press, 2009.

Jørgensen, N. O., Laier, T., Buchardt, B., and Cederberg, T.: Shallow hydrocarbon gas in the nothern Jutland-Kattegat region, Denmark, Bull. Geol. Soc, 38, 69-76, 1990.

Loeng, H.: Features of the physical oceanographic conditions of the Barents Sea, Polar Research, 10, 5-18, doi:10.3402/polar.v10i1.6723, 1991.
Marín-Moreno, H., Minshull Timothy, A., Westbrook Graham, K., Sinha, B., and Sarkar, S.: The response of methane hydrate beneath the seabed offshore Svalbard to ocean warming during the next three centuries, Geophysical Research Letters, 40, 5159-5163, doi:10.1002/grl.50985, 2013.
McDougall, T. J., and Barker, P. M.: Getting started with TEOS-10 and the Gibbs Seawater (GSW) oceanographic toolbox, SCOR/IAPSO WG, 127, 1-28, 2011.
McGinnis, D., Greinert, J., Artemov, Y., Beaubien, S., and Wüest, A.: Fate of rising methane bubbles in stratified waters: How much methane reaches the atmosphere?, Journal of Geophysical Research: Oceans (1978–2012), 111, doi:10.1029/2005JC003183, 2006.
Medwin, H., and Clay, C. S.: Fundamentals of acoustical oceanography, Academic press, 1997.
Miller, C. M., Dickens, G. R., Jakobsson, M., Johansson, C., Koshurnikov, A., O'Regan, M., Muschitiello, F., Stranne, C., and Mörth, C. M.: Pore water geochemistry along continental slopes north of the East Siberian Sea: inference of low methane concentrations, Biogeosciences, 14, 2929-2953, doi:10.5194/bg-14-2929-2017, 2017.
Myhre, C. L., Ferré, B., Platt, S. M., Silyakova, A., Hermansen, O., Allen, G., Pisso, I., Schmidbauer, N., Stohl, A., and Pitt, J.: Extensive release of methane from Arctic seabed west of Svalbard during summer 2014 does not influence the atmosphere, Geophysical Research Letters, 43, 4624-4631, doi:10.1002/2016GL068999, 2016.
Ostrovsky, I.: Methane bubbles in Lake Kinneret: Quantification and temporal and spatial heterogeneity, Limnology and Oceanography, 48, 1030-1036, doi:10.4319/lo.2003.48.3.1030, 2003.
Ostrovsky, I., McGinnis, D. F., Lapidus, L., and Eckert, W.: Quantifying gas ebullition with echosounder: the role of methane transport by bubbles in a medium-sized lake, Limnology and Oceanography: Methods, 6, 105-118, doi:10.4319/lom.2008.6.105, 2008.
Platt, S. M., Eckhardt, S., Ferré, B., Fisher, R. E., Hermansen, O., Jansson, P., Lowry, D., Nisbet, E. G., Pisso, I., Schmidbauer, N., Silyakova, A., Stohl, A., Svendby, T. M., Vadakkepuliyambatta, S., Mienert, J., and Lund Myhre, C.: Methane at Svalbard and over the European Arctic Ocean, Atmos. Chem. Phys., 18, 17207-17224, doi:10.5194/acp-18-17207-2018, 2018.
Pohlman, J. W., Greinert, J., Ruppel, C., Silyakova, A., Vielstädte, L., Casso, M., Mienert, J., and Bünz, S.: Enhanced CO₂ uptake at a shallow Arctic Ocean seep field overwhelms the positive warming potential of emitted methane, Proceedings of the National Academy of Sciences, 114, 5355, doi:10.1073/pnas.1618926114, 2017.
Portnov, A., Vadakkepuliyambatta, S., Mienert, J., and Hubbard, A.: Ice-sheet-driven methane storage and release in the Arctic, Nature Communications, 7, 10314, doi:10.1038/ncomms10314 https://www.nature.com/articles/ncomms10314#supplementary-information, 2016.
Reagan, M. T., Moridis, G. J., Elliott, S. M., and Maltrud, M.: Contribution of oceanic gas hydrate dissociation to the formation of Arctic Ocean methane plumes, Journal of Geophysical Research: Oceans, 116, doi:10.1029/2011JC007189, 2011.
Reeburgh, W. S.: Oceanic Methane Biogeochemistry, Chemical Reviews, 107, 486-513, doi:10.1021/cr050362v, 2007.
Ruppel, C. D., and Kessler, J. D.: The Interaction of Climate Change and Methane Hydrates, Reviews of Geophysics, doi:10.1002/2016RG000534, 2016.
Sahling, H., Römer, M., Pape, T., Bergès, B., dos Santos Fereirra, C., Boelmann, J., Geprägs, P., Tomczyk, M., Nowald, N., and Dimmler, W.: Gas emissions at the continental margin west of Svalbard: mapping, sampling, and quantification, Biogeosciences, 11, 6029-6046, doi:10.5194/bg-11-6029-2014, 2014.
Schauer, U., Fahrbach, E., Osterhus, S., and Rohardt, G.: Arctic warming through the Fram Strait: Oceanic heat transport from 3 years of measurements, Journal of Geophysical Research: Oceans, 109, doi:10.1029/2003JC001823, 2004.
Shakhova, N., Semiletov, I., Salyuk, A., Yusupov, V., Kosmach, D., and Gustafsson, Ö.: Extensive Methane Venting to the Atmosphere from Sediments of the East Siberian Arctic Shelf, Science, 327, 1246-1250, doi:10.1126/science.1182221, 2010.
Shakhova, N., Semiletov, I., Leifer, I., Sergienko, V., Salyuk, A., Kosmach, D., Chernykh, D., Stubbs, C., Nicolsky, D., Tumskoy, V., and Gustafsson, O.: Ebullition and storm-induced methane release from the East Siberian Arctic Shelf, Nature Geosci, 7, 64-70, doi:10.1038/ngeo2007, 2014.
Skogseth, R., Haugan, P. M., and Jakobsson, M.: Watermass transformations in Storfjorden, Continental Shelf Research, 25, 667-695, doi:10.1016/j.csr.2004.10.005, 2005.
Ślubowska-Woldengen, M., Rasmussen, T. L., Koç, N., Klitgaard-Kristensen, D., Nilsen, F., and Solheim, A.: Advection of Atlantic Water to the western and northern Svalbard shelf since 17,500calyr BP, Quaternary Science Reviews, 26, 463-478, doi:10.1016/j.quascirev.2006.09.009, 2007.
Sommer, S., Schmidt, M., and Linke, P.: Continuous inline mapping of a dissolved methane plume at a blowout site in the Central North Sea UK using a membrane inlet mass spectrometer – Water column stratification

impedes immediate methane release into the atmosphere, Marine and Petroleum Geology, 68, 766-775, 10.1016/j.marpetgeo.2015.08.020, 2015.
Stashchuk, N., Vlasenko, V., Inall, M. E., and Aleynik, D.: Horizontal dispersion in shelf seas: High resolution modelling as an aid to sparse sampling, Progress in Oceanography, 128, 74-87, doi:10.1016/j.pocean.2014.08.007, 2014.
Steinle, L., Graves, C. A., Treude, T., Ferré, B., Biastoch, A., Bussmann, I., Berndt, C., Krastel, S., James, R. H., Behrens, E., Böning, C. W., Greinert, J., Sapart, C.-J., Scheinert, M., Sommer, S., Lehmann, M. F., and Niemann, H.: Water column methanotrophy controlled by a rapid oceanographic switch, Nature Geoscience, 8, 378, doi:10.1038/ngeo2420, 2015.
https://www.nature.com/articles/ngeo2420#supplementary-information, 2015.
Sundermeyer, M. A., and Ledwell, J. R.: Lateral dispersion over the continental shelf: Analysis of dye release experiments, Journal of Geophysical Research: Oceans, 106, 9603-9621, doi:10.1029/2000JC900138, 2001.
Tishchenko, P., Hensen, C., Wallmann, K., and Wong, C. S.: Calculation of the stability and solubility of methane hydrate in seawater, Chemical geology, 219, 37-52, doi:10.1016/j.chemgeo.2005.02.008, 2005.
Veloso, M., Greinert, J., Mienert, J., and De Batist, M.: A new methodology for quantifying bubble flow rates in deep water using splitbeam echosounders: Examples from the Arctic offshore NW-Svalbard, Limnology and Oceanography: Methods, 13, 267-287, doi:10.1002/lom3.10024, 2015.
Veloso, M., Greinert, J., Mienert, J., and De Batist, M.: Corrigendum: A new methodology for quantifying bubble flow rates in deep water using splitbeam echosounders: Examples from the Arctic offshore NW-Svalbard, Limnology and Oceanography: Methods, 17, 177-178, doi:10.1002/lom3.10313, 20192019a.
Veloso, M., Jansson, P., De Batist, M., Minshull, T. A., Westbrook, G. K., Pälike, H., Bünz, S., Wright, I., and Greinert, J.: Variability of acoustically evidenced methane bubble emissions offshore western Svalbard, Geophysical Research Letters, 10.1029/2019GL082750 2019b.
Wankel, S. D., Joye, S. B., Samarkin, V. A., Shah, S. R., Friederich, G., Melas-Kyriazi, J., and Girguis, P. R.: New constraints on methane fluxes and rates of anaerobic methane oxidation in a Gulf of Mexico brine pool via in situ mass spectrometry, Deep Sea Research Part II: Topical Studies in Oceanography, 57, 2022-2029, 10.1016/j.dsr2.2010.05.009, 2010.
Weber, T. C., Mayer, L., Jerram, K., Beaudoin, J., Rzhanov, Y., and Lovalvo, D.: Acoustic estimates of methane gas flux from the seabed in a 6000 km2 region in the Northern Gulf of Mexico, Geochemistry, Geophysics, Geosystems, 15, 1911-1925, doi:10.1002/2014GC005271, 2014.
Westbrook, G. K., Thatcher, K. E., Rohling, E. J., Piotrowski, A. M., Pälike, H., Osborne, A. H., Nisbet, E. G., Minshull, T. A., Lanoisellé, M., and James, R. H.: Escape of methane gas from the seabed along the West Spitsbergen continental margin, Geophysical Research Letters, 36, doi:10.1029/2009GL039191, 2009.
Wiesenburg, D. A., and Guinasso, J. N. L.: Equilibrium solubilities of methane, carbon monoxide, and hydrogen in water and sea water, Journal of Chemical and Engineering Data, 24, 356-360, doi:10.1021/je60083a006, 1979.

Table 1: Average concentrations (nmol l^{-1}) calculated with different methods at different altitudes as indicated in the first column (metres above the seabed, masf). [1]Average of the sparse discrete sampling. [2]Average of high-resolution (MILS) measurements. [3]Average of linearly interpolated concentrations based on discrete measurements. [4]Average concentrations from the 2D model, extracted from depths matching the MILS position. [5]Average concentrations within the box (4500 m (L) × 50 m (W) × 75 m (H)) based on the high-resolution measurements or interpolated concentrations along the box, the vertical dissolution-profile, and the mean horizontal concentration gradient across the width of the box. [6]Average of the 2D model best simulation result from 0–75 masf. [7]The CV model yields a box value only.

Dataset	Discrete	High-resolution	Box
MILS ~15 masf	-	47[2]	22[5]
DS ~5 masf	104[1]	108[3]	39[5]
DS ~15 masf	77[1]	77[3]	29[5]
DS ~25 masf	44[1]	49[3]	20[5]
2D model (~15[4] and 0–75[6] masf)	-	60[4]	22[6]
CV model	-	-	23[7]